Development of a Novel Palladium Membrane-based Alkaline Direct Methanol Fuel Cell

A Major Qualifying Project Report:

submitted to

the Faculty of the WORCESTER POLYTECHNIC INSTITUTE

Chemical Engineering Department

in partial fulfillment of the requirements

for the Degree of Bachelor of Science

by

Brian Walker

Date: April 25th, 2013

Advisor: Ravindra Datta

Acknowledgements

I would like to thank the entire fuel cell lab group at Worcester Polytechnic Institute for assisting me in the completion of this project.

I would like to especially thank my advisor, Professor Ravi Datta and graduate student Susan Yen for working with me throughout the duration of this project and offering excellent advice and insight into the concepts and tasks encountered while working on this project.

Abstract

The conventional direct methanol fuel cell (DMFC) operates with Nafion® membrane at ambient temperatures using dilute methanol feeds, and provides relatively poor performance because of slow kinetics and methanol crossover, despite high catalyst loading. The alternative is to reform methanol in a reformer and use it in conjunction with a hydrogen-oxygen PEM fuel cell, which results in a bulky unit. In this project, the overall goal was to design a high temperature DMFC based on alkaline electrolyte that could utilize concentrated methanol feeds directly. It uses a palladium membrane that serves both as the anode and as a membrane that precludes methanol crossover as well as CO_2 reaction with the alkaline electrolyte.

This novel fuel cell is designed as a planar cell, with the SiC ceramic support oriented as a circular wafer. This support had a dense palladium and silver membrane plated on one of its circular faces, operating as the anode. The other face of the support was plated in silver as the porous cathode. This "chip" was positioned in a Swagelok® fixture which was connected to feed tubes for the fuel flow. All contact between the electrodes and the metal fixture was insulated to prevent short-circuiting. Teflon ferrules and Teflon tape were used for insulation. Silver wire was attached to each node to connect to the external circuit. Spongy gaskets were used to seal the support and prevent cracking. A porous nickel oxide plate was also placed on one side of the support, separated by a gasket, to help support entire fixture.

The chief accomplishment in this work was to establish an effective method of fabrication of a dense Pd/Ag membrane on the SiC ceramic support, which is the crux of this fuel cell. Problems with the activation of the ceramic support surface were overcome and the plating and annealing processes were improved to reduce time and to optimize the process. When operating the fuel cell using pure hydrogen feed instead of methanol, the cell was able to generate a voltage thus showing promising signs that the performance achieved here could be improved upon. The next step for this research and experimentation is to fine-tune the fabrication procedure using the recommendations made in this report and then attempt to operate the fuel cell using a methanol feed.

Table of Contents

Table of Figures

1. Introduction

The world runs on a variety of energy sources. Of these sources, the most predominant, petroleum and other fossil fuels, are nonrenewable. This means that once the supply has been consumed, no more will appear on this earth. As we run out of these fuels, it will become more and more imperative to find renewable alternatives that can power the next generation. These sources include solar, wind, and hydro power, as well as biofuel and biomass. Currently, approximately 10% of the world's energy consumption comes from renewable sources while approximately 80% of the United States' energy consumption comes from fossil fuels (U.S. Energy Information Administration, 2013). The growing concern with fossil fuels is that they are not renewable and have high carbon emissions. These "greenhouse gases" get released into the atmosphere and trap heat from escaping, the primary cause of climate change. Increasing the efficiency of the heat engine utilizing the fuel will reduce these emissions, however.

Fuel cells produce electricity directly from a fuel but can do so at a higher efficiency, thus reducing emissions. The higher efficiency proportionately reduces the emissions of CO_2 from fuel, both fossil and renewable. A fuel cell takes energy from chemicals and turns it into electricity through a chemical reaction. This electricity can then be directed outside of the cell via conductive wiring and used to power a separate process. The reaction occurs at the anode, which is the negatively-charged electrode. It leads to the release of electrons, which travel through the external circuit to provide energy for another device. After passing through the outside circuit, where useful work is extracted from them, the electrons return to the cell at the cathode, which is the positively-charged electrode of the cell. There the electrons drive another reaction, the products of which travel through an appropriate electrolyte and continue to drive the reaction at the anode. An electrolyte is inserted into the system between the two electrodes which allows for the ions produced at either the anode or the cathode to travel between them.

These cells can be very valuable because they can directly utilize reactant chemicals such as methanol and hydrogen gas which may be produced from fossil or renewable fuels. Many, in fact, run on hydrogen gas and oxygen. Those that can run on pure hydrogen as a fuel source will

then only release heat and water vapor into the atmosphere. Additionally, fuel cells have a much higher efficiency than common internal combustible engines. Figure 1 diagrams the comparison between the efficiency of a phosphoric acid fuel cell and other common energy conversion systems.

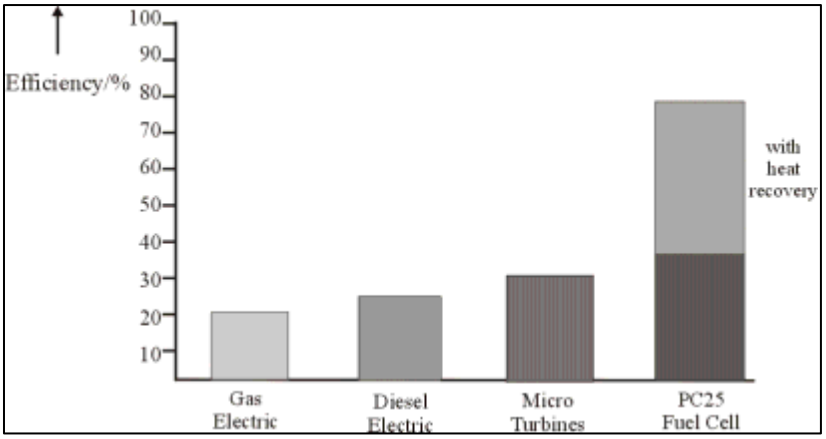

Figure 1: Efficiency comparison of a PAFC vs. other conventional energy conversions (Datta, Fuel Cells, 2013)

Direct methanol fuel cells are those that run on methanol or a methanol – water solution. These cells can be less expensive because reformation of the fuel is not necessary and they operate at relatively low temperatures. The hydrogen atoms that drive the chemical reaction in the cell come from the methanol instead of hydrogen gas. There is also an added convenience in that methanol can be stored and transported as a liquid.

For this MQP project, we attempted to create and test a direct methanol fuel cell, but with several modifications from the status quo. What makes this type of cell different from many other types of cells is that it runs on methanol-water solution that gets reformed on a Pd-Ag membrane. The hydrogen gas that is produced crosses through the palladium membrane as monatomic hydrogen atoms. These atoms react with OH^- ions along the Pd membrane – electrolyte interface, producing H_2O and releasing electrons. The Pd membrane acts as a barrier for the CO_2 produced at the anode, preventing it from coming in contact with the electrolyte and poisoning it. This is what will allow us to utilize the alkaline electrolyte while still operating with methanol fuel. The motivation behind this is that we can reduce our operating costs by

using a convenient and inexpensive liquid fuel while still achieving relatively high efficiencies, similar to H_2-O_2 alkaline fuel cells. A schematic for the proposed cell is shown in Figure 2.

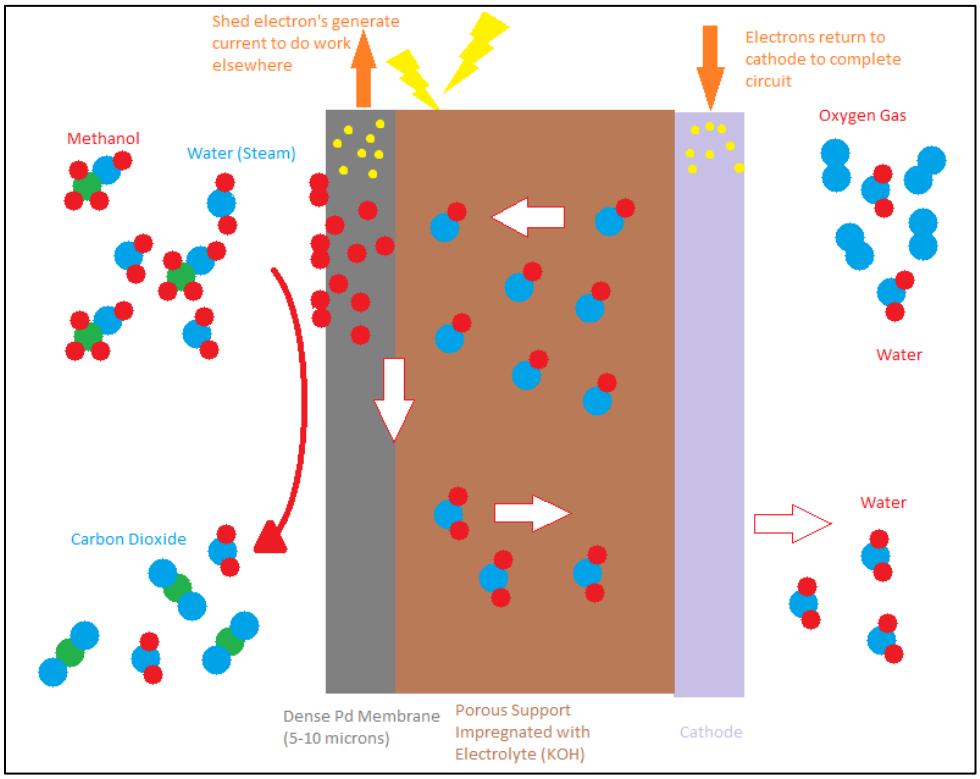

Figure 2: Proposed Novel Fuel Cell Schematic

As shown in Figure 2, methanol and water vapor contact the cell at the anode, while oxygen contacts the cell at the cathode, and carbon dioxide and water are the products. The hydroxide ions travel through the electrolyte, which is characteristic of alkaline fuel cells.

We worked to prepare the individual pieces of the fuel cell, assemble them into one single unit, and test the fuel cell for its feasibility, energy output, and efficiency. In order to accomplish this goal, many preparation steps were necessary. Prior to assembly, the SiC ceramic supports for the electrodes and the electrolyte needed to undergo much preparation. They were tested to determine each support's porosity and how well they could soak up the chosen electrolyte, potassium hydroxide. Then the circular faces of each chip were seeded with palladium nuclei during an activation step. This would allow for electroless plating of each side of the support, which would then become the electrodes for each cell. This plating was made possible by the

palladium nuclei that were planted onto the surfaces and attracted palladium and silver atoms to be deposited there as well.

After several rounds of plating, alternating between palladium plating and silver plating until the desired Pd/Ag ratio was achieved, the ceramic “chips” were annealed in an oven to create a Pd/Ag alloy on one side of the chip. From this point the cells could be assembled. The final cell was tested utilizing H_2 and oxygen to get a baseline and determine whether the cell was operational. Once troubleshooting is complete, it should be tested again using methanol in place of the hydrogen to test it as a DMFC.

For this MQP project, the focus was directed at the fabrication of the cell as well as testing its feasibility by running it with hydrogen gas. The feasibility of this novel direct methanol fuel cell was investigated and the initial results were promising. This report will explain the background research that went into learning about the various fuel cell elements involved with this novel cell. It will also give detailed accounts of both the design of the cell and the procedural steps taken in creating the final design. The results of our tests, including preliminary tests which helped determine the most effective way to prepare the fuel cell prior to operation, will be discussed, along with recommendations for future work.

2. Literature Review

What is a Fuel Cell?

Since its first demonstration in 1839, by Sir William Grove, the fuel cell has been developed and its design fine-tuned. Despite a history that ranges back nearly 200 years, however, the technology always seems to remain "five years away from commercial exploitation" because of technological and cost challenges (How Fuel Cells Work, 5). Fuel cells are devices that can produce electrical energy from a chemical reaction. A chemical reaction takes place at one of the electrodes, i.e., the anode, which releases electrons. These electrons move through a circuit and this current is used to perform useful work. It converts chemical energy into electrical energy. As Grove's early experiments strongly suggested, hydrogen and oxygen, which are examples of a fuel and an oxidant, respectively, are attractive reactants (History, 2004). Most modern-day fuel cells still utilize these two gases as their fuel and oxidant.

The main components of a fuel cell are as follows: a cathode, an anode, an electrolyte, and an external circuit through which an electrical current can leave the cell and perform work elsewhere. This current is generated through the chemical reactions that occur at the electrodes, causing the shedding of electrons by the fuel source at the anode. The anode is the electrode at which the fuel is oxidized, which causes the shedding of electrons. Hydrogen is the most common fuel. It enters the fuel cell on the anode side and dissociates into H^+ ions and electrons. The electrons move through the external circuit, creating an electrical current, while the H^+ ions react with other compounds. Depending on the type of fuel cell, these H^+ ions will either pass through the electrolyte or stay at the anode. Fuel cells that require the passage of these ions through the electrolyte fall under a group called proton exchange fuel cells. Fuel cells that don't allow the passage of these protons utilize the movement of different ions from the cathode to the anode, where they then can react with the hydrogen atoms. Several of these different fuel cells will be discussed in the later sections but all require this flow of electrons through the external circuit to perform useful work.

When the electrons return to the cell, at the cathode, they drive yet another chemical reaction and this cyclical rotation maintains the electrical output of the cell. The cathode is the

electrode where oxygen reduction takes place. This reduction requires the electrons that were shed via the reaction at the anode (Electrode, 2013). The oxygen supplied at the cathode may either come from a pure O_2 feed or from air.

The electrolyte is an important part of the cell because it only permits the appropriate ions to pass between the electrodes. These ions are charge-carrying particles that pass through the electrolyte and drive the reactions at the electrodes. In different types of fuel cells, different ions may pass through the electrolyte. In an alkaline fuel cell, for example, OH^- ions pass from the cathode to the anode, oxidizing the dissociated hydrogen ions, which then leads to the shedding of electrons. However, in a polymer electrolyte membrane fuel cell, it is H^+ ions moving from the anode to the cathode that allow for the circuit to be completed. The passage of the incorrect ions, atoms, or free electrons would disrupt the chemical process (History, 2004).

Polymer Electrolyte Membrane Fuel Cell

Also known as a proton exchange membrane fuel cell, the PEM fuel cell was first developed in 1955 by William Grubb while working for General Electric (Datta, Fuel Cells, 2013). Since this first design, PEM fuel cells have grown rapidly. The design of the electrolyte revolutionized the fuel cell industry by bonding the acid electrolyte to a polymer, creating a solid membrane. This solid membrane, combined with good efficiency capabilities (<60%), have contributed to the growth of the PEM fuel cell (Singh, 2008). Many alternatives to the PEM design, e.g., phosphoric acid fuel cells or molten carbonate fuel cells, utilize a porous support layer in which the liquid electrolyte is held in place through cohesive and capillary forces. However, over time the electrolyte is susceptible to movement, which reduces performance and causes corrosion. The polymer electrolyte membrane helps avoid some of these issues by holding the electrolyte in place via covalent bonding (Datta, Fuel Cells, 2013). This membrane is also flexible, which helps limit leaks and cracks.

In PEMFC's, gas diffusion layers (GDL's) are placed on the outside of both electrodes. These layers function both to manage the moisture within the cell and also allow the fuel gas to pass through to the electrodes. The GDL's needed to prevent flooding of the cell while also

maintaining a relatively high humidity. This is controlled by the both pore size and the concavity or convexity of the pores (L. Cindrellam, 2009). Because such a delicate balance is required, these layers must be precisely constructed and selected. They also can assist in providing mechanical strength for the cell. Figure 3 provides a schematic for a PEM fuel cell.

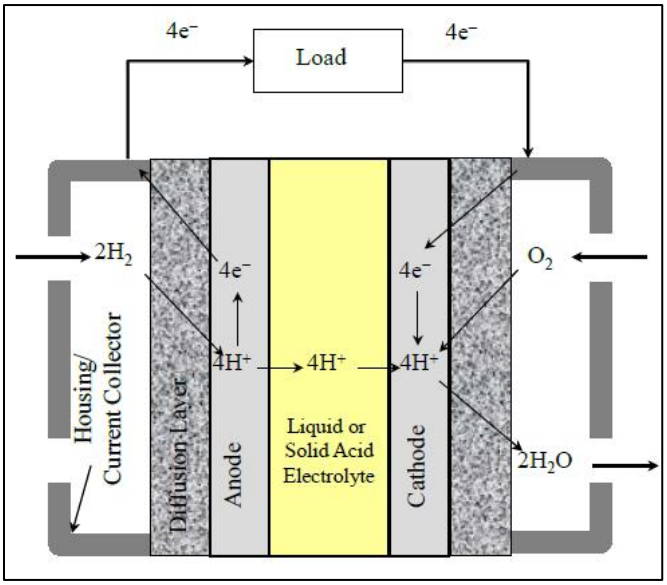

Figure 3: PEM Fuel Cell (Datta, 2012)

On the anode, a platinum catalyst causes the dissociation of the H_2 fuel into protons (H^+ ions) and electrons. The polymer membrane, for which the cell is named, only permits passage of the protons through it, while the negatively-charged electrons must move through the external circuit. The protons move through the cell to the cathode, reacting with the incoming oxygen gas and form water, using the electrons that return from the circuit.

PEM fuel cells require purified hydrogen and oxygen gas or air streams and can operate around 80˚C or less. Because of this low operating temperature, these cells are suitable for vehicles and homes (History, 2004). The overall reaction and the reactions at each electrode of the cell are

$$\begin{aligned} Anode: &\quad \mathrm{H_2} \leftrightarrow 2\mathrm{H^+} + 2\mathrm{e^-} \\ Cathode: &\quad {}^1\!/_2\,\mathrm{O_2} + 2\mathrm{H^+} + 2\mathrm{e^-} \leftrightarrow \mathrm{H_2O} \\ Overall: &\quad \mathrm{H_2} + {}^1\!/_2\,\mathrm{O_2} \leftrightarrow \mathrm{H_2O} \end{aligned}$$

These reactions demonstrate the movement of the H^+ ions moving through the electrolyte from one electrode to the other (Datta, PEM Fuel Cell/ DMFC Principles, 2012). This is important for the functioning of the cell, but again it is important that the membrane doesn't allow either gas to pass through because it would ruin the cell's performance. A plot of the performance for a PEM fuel cell can be seen in Figure 4.

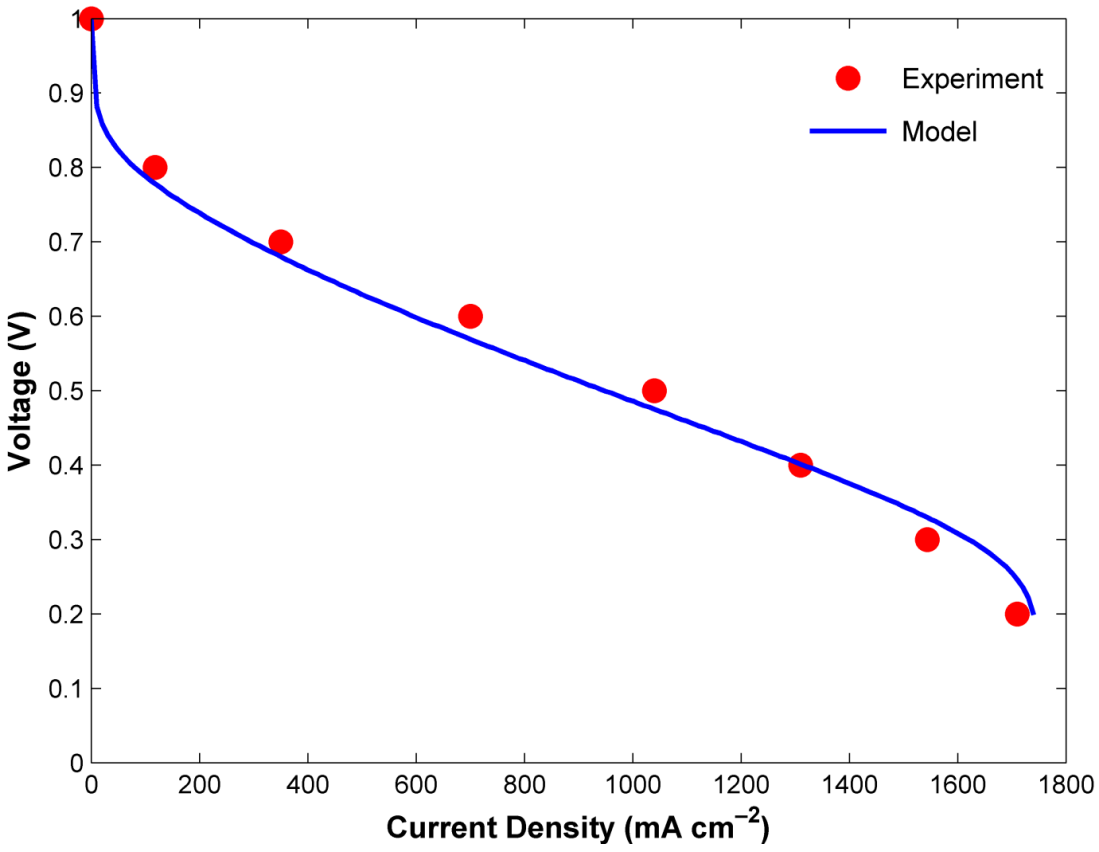

Figure 4: Performance plot for a single PEM fuel cell

As the plot shows, the voltage decreases as the current density for the circuit increases. The curve of the graph shows the electrochemical efficiency for a given current density. In an ideal scenario, the voltage would maintain its initial value, in this case 1.0 V, for all current densities. This initial value, called the Open Circuit Voltage, or OCV, is the voltage reading for a cell with no current being drawn. Unfortunately, ideal conditions are not feasible and every cell performance plot will trend downward like this one.

Alkaline Fuel Cell

An alkaline fuel cell is another type of cell that also runs on pure hydrogen and oxygen. AFC's have the highest electrical efficiencies of all fuel cells, reaching up to 70% (Carrette, Friedrich, & Stimming, 2001). These fuel cells get their names because the electrolyte used for these fuel cells is an aqueous alkaline solution containing potassium hydroxide (KOH). Alkaline fuel cells were some of the first to be developed. The older high-temperature alkaline fuel cells can operate between 100 ˚C and 250 ˚C, but newer designs operate at a much lower range: between 23 ˚C and 70 ˚C (U.S. Department of Energy, 2011). This lower temperature range is possible because the potassium hydroxide electrolyte provides much faster electrode kinetics than an acid electrolyte. This means that the electrode losses are smaller. However, higher operation temperatures are still advantageous for improved kinetics (Carrette, Friedrich, & Stimming, 2001).

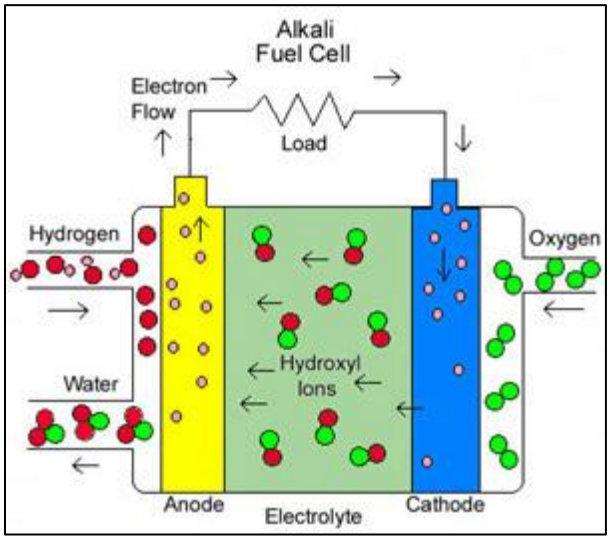

Figure 5: Alkaline Fuel Cell (History, 2004)

Because of their alkaline electrolyte as opposed to the acid electrolyte of a PEM fuel cell, hydroxyl ions (OH^-) are produced at the cathode and travel to the anode to carry the charge through the electrolyte (Carrette, Friedrich, & Stimming, 2001). These hydroxyl ions react with the hydrogen gas fuel, shedding electrons and creating water molecules. These electrons travel through the external circuit to the cathode, where they help drive a reaction between the

incoming oxygen gas and water to make hydroxyl groups. These ions then move to the anode and the process continues. The reactions that occur for an alkaline fuel cell are:

$$Anode: \quad H_2 + 2OH^- \rightarrow 2H_2O + 2e^-$$

$$Cathode: \quad O_2 + 2H_2O + 4e^- \rightarrow 4OH^-$$

$$Overall: \quad H_2 + O_2 + 2e^- \rightarrow 2OH^-$$

The reason that these cells need to run on purified hydrogen and oxygen gas streams is because gases like carbon dioxide can contaminate the electrolyte and eventually ruin the cell. The CO_2 reacts with the OH^- ion in the aqueous solution to form HCO_3^- and over time this reaction degrades the fuel cell performance (Welge, 1940). The additional cost of electrolyte replacement and the expensive platinum electrode catalysts are considered major downsides to these types of cells (Carrette, Friedrich, & Stimming, 2001). Since the electrolyte contamination is easy, the frequency of replacement is higher than other cells types (U.S. Department of Energy, 2011). Also, because of their liquid electrolytes, leaking can be a concern. These fuel cells have been used for power on space crafts, although terrestrial applications based on air are more challenging because of the presence of CO_2. For these reasons they also cannot use carbonaceous fuels such as methanol. Figure 6 demonstrates the effect of the presence of carbon dioxide on the fuel cell's performance over time.

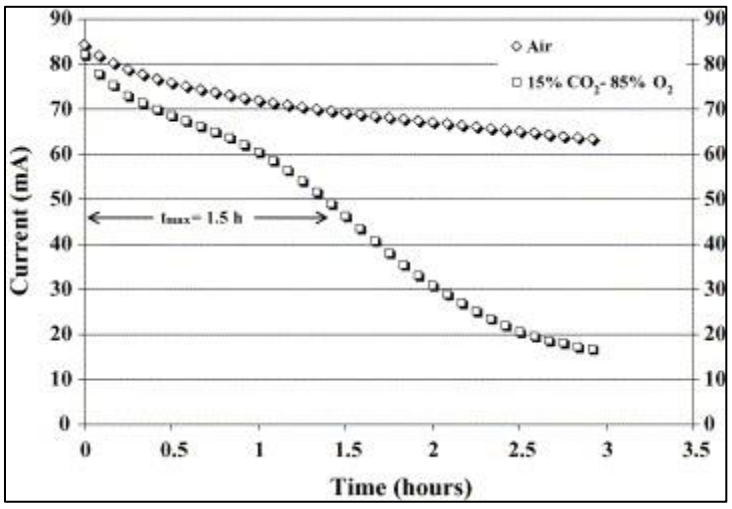

Figure 6: Cell current versus time for two fuels: air and a CO_2-O_2 mixture (A. Tewari, 2006)

As the graph indicates, crossover of the fuel gases through the electrolyte reduces performance level over time. It also illustrates how the presence of CO_2 reduces the overall performance of the cell. Air, which contains .03% carbon dioxide by volume, has a significantly higher current than the 15% carbon dioxide mixture and is able to sustain this higher current over time. The performance of the air-driven experiment could be improved still if pure hydrogen was used instead. Because of this sensitivity to carbon, these fuel cells need to be run on pure hydrogen or are subject to frequent electrolyte replacements. The plot in Figure 7 shows the improved performance of an alkaline fuel cell when run on pure hydrogen.

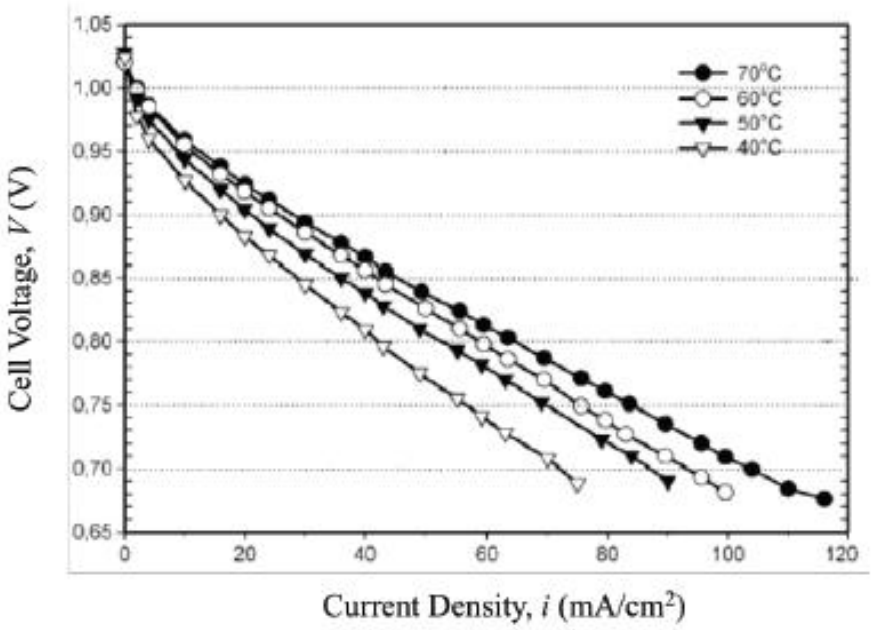

Figure 7: Alkaline fuel cell performance at varying temperatures (Datta, Fuel Cells, 2013)

Relative to other fuel cells, AFC's have the best efficiency and performance, which made them an attractive option to investigate while designing our novel cell.

Direct Methanol Fuel Cell

A direct methanol fuel cell (DMFC) operates using methanol and oxygen from air as its reactants. A schematic for a DMFC is shown in Figure 8.

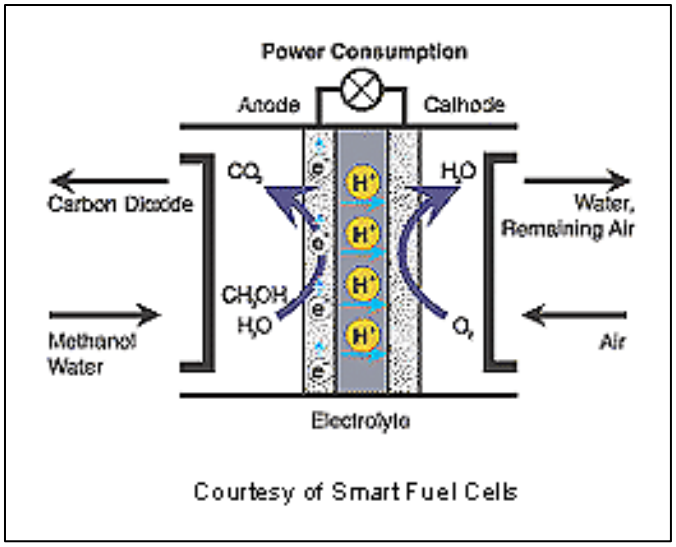

Figure 8: Direct Methanol Fuel Cell Diagram (NFCRC, 2009)

The chemical reactions taking place at the electrodes and the overall reaction are as follows:

$$Anode: \quad CH_3OH + H_2O \rightarrow 6H^+ + 6e^- + CO_2$$

$$Cathode: \quad {}^3/_2\, O_2 + H^+ + 6e^- \rightarrow 3H_2O$$

$$Overall: \quad CH_3OH + {}^3/_2\, O_2 \rightarrow 2H_2O + CO_2$$

These fuel cells are an attractive option because of their low operating temperatures (<80 ˚C) and the use of methanol as a fuel. Unlike other fuel cells, purification of a hydrogen fuel isn't necessary and saves on cost of operation. Methanol is also a good fuel option because it is easily stored, inexpensive, and can be derived from either natural gas or biomass resources. Because methanol can be a liquid or a gas depending on the operating temperature, DMFC's can operate on either liquid or gaseous methanol/methanol mixtures (Carrette, Friedrich, & Stimming, 2001). There are also *Indirect* Methanol Fuel Cells (IMFC's), which utilize methanol as a fuel source as well. IMFC's need to reform the methanol gas before feeding it into the PEM fuel cell. However, this is an added stage in the power plant and an added expense.

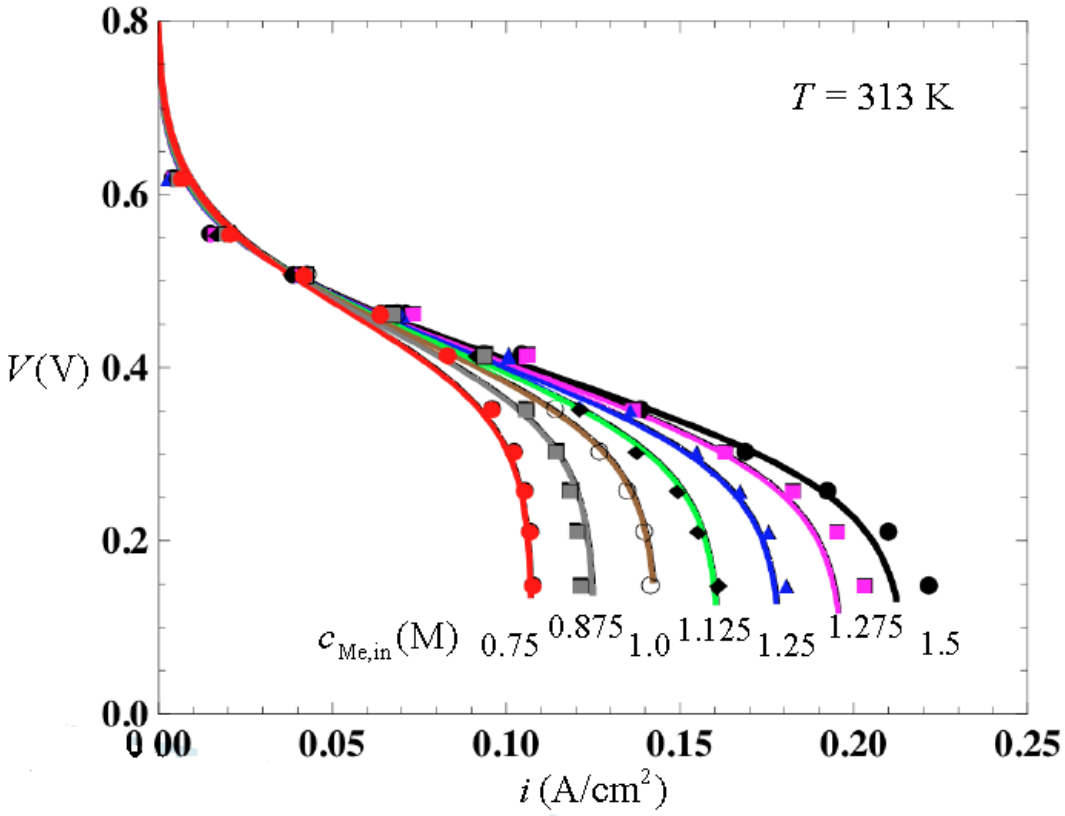

Figure 9: Performance plot of a DMFC for various methanol feed concentrations (Datta, PEM Fuel Cell/ DMFC Principles, 2012)

Figure 9 shows the performance of a DMFC for various methanol concentrations in the feed. As illustrated, increased levels of methanol in the feed reduce the performance of the cell because they are susceptible to methanol crossover. When methanol crosses over to the cathode, it has a significant negative effect on the oxygen reduction reaction, reducing cell efficiency (C.Y. Du, 2007). When this data is compared to that of the PEM fuel cell, one can see that direct methanol fuel cells perform at a much lower level. If the performance of these fuel cells could be improved, they would a cheaper alternative to PEM and alkaline fuel cells.

The DMFC is based on membrane technology similar to that in the PEM fuel cells. A goal of the membrane is to increase the proton transport between the electrodes via the electrolyte and also to prevent methanol cross-over. With methanol crossover, methanol molecules diffuse through the membrane at the anode and cross the electrolyte into the cathode, which results in a decreased cell performance. The ultimate goal would be to create a membrane that could prevent methanol diffusion while still allowing for proton exchange. One example would be the

work of W.C. Choi, of the Chemical Engineering Department at the Korea Advanced Institute of Science and Technology. Choi and his colleagues were working to use surface etching and palladium sputtering to reduce the pore size of the membrane and thus help reduce methanol cross-over in DMFC's (Choi, Kim, & Woo, 2001).

Reformers and PEM Fuel Cells

Because PEM fuel cells require a pure hydrogen stream, a reformer is necessary to convert a source such as methanol into hydrogen gas in an indirect methanol fuel cell. This is accomplished by heating the methanol to a high temperature (>250 ˚C) along with steam. These reactants reform via the reaction $CH_3OH + H_2O \rightarrow CO_2 + 3H_2$ (Gernand, 2007).

This step greatly increases the cost of operation and is a major limitation. Only roughly 10 ppm carbon monoxide is allowable in the feed for fuel cells that operate below 80 ˚C (Datta, Fuel Cells, 2013). Anything greater and the performance of the cell is significantly compromised. Any reforming that is performed prior to fuel injection into the cell must have steps to greatly cut down the amount of CO in the feed stream. Figure 10 gives a basic diagram of how a cell operating with a fuel reformer would look. The relative size of the reformer versus the actual fuel cell and the presence of a heat source both make this process much more expensive.

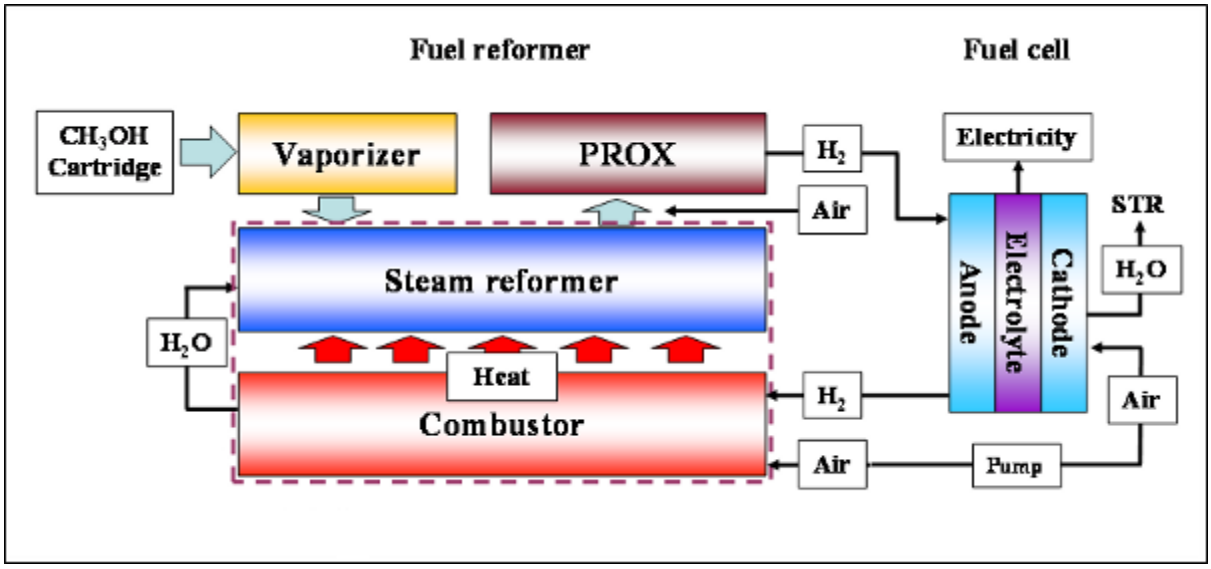

Figure 10: Fuel Cell Process Utilizing a Fuel Reformer (Kim, 2009)

As shown in Figure 10, the methanol enters the system and is vaporized. Next it enters the steam reformer where the reaction occurs and carbon dioxide and hydrogen are produced. The presence of a catalyst or a semi-permeable membrane allows this to happen, removing the hydrogen from the methanol fuel. Next it exits the reformer and can then be used by the cell. The hydrogen that exits the fuel cell unreacted can be recycled as a combustible gas to heat the reformer.

Palladium Membranes

A palladium membrane may be used for purifying H_2 either after the reformer or integrated into the reformer. This is made by depositing palladium as a thin dense film onto a solid support in order to allow H_2 passage but restrict the diffusion of other gases through it. It can be prepared through an electroless plating technique on a support by first seeding the support surface and then being bathed in a plating solution. In order to activate the surface, several rounds of seeding are performed to deposit palladium nuclei onto the surface, which aid in the plating of palladium in the later process. These nuclei initiate autocatalytic reduction of a palladium salt in the plating solution, resulting in deposition. For optimal results, between 4 and 10 activation cycles should be completed (Mardilovich, She, & Ma, 1998).

Dense membranes are well suited for high-temperature hydrogen separations. Figure 11 shows hydrogen passage through a Pd/Ag membrane.

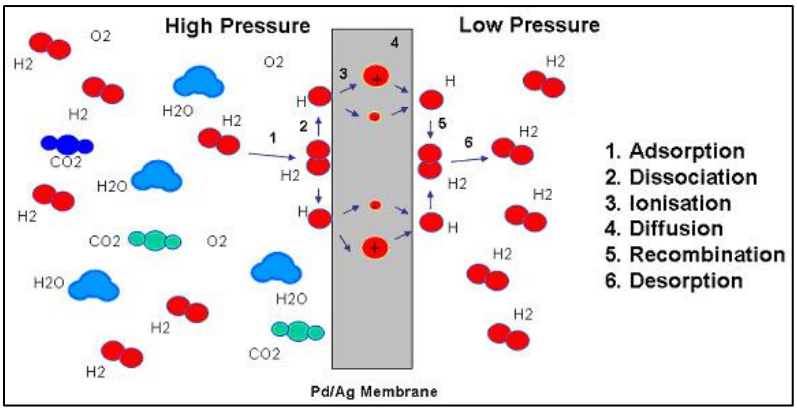

Figure 11: Hydrogen diffusion through a Pd/Ag Membrane (Palladium Membrane Purification, 2013)

Hydrogen gas adsorbs on the surface of the membrane, then dissociates into monatomic hydrogen. These atoms, which are small enough to pass through the pores of the membrane, diffuse through because of a pressure gradient, dissociating further into protons and electrons. Once they pass through onto the other side, they quickly reform hydrogen gas. The important aspect of this membrane is that the pores are too small for contaminants, such and CO_2 and H_2O to pass through.

Porous stainless steel is a common support choice because it is resistant to cracking and its thermal expansion coefficient is almost identical to that of palladium (Mardilovich, She, & Ma, 1998). The membrane will prevent unwanted molecules from passing through the cell into the electrolyte. Data shown in Figure 12 demonstrates how a palladium membrane can allow permeance of hydrogen gas but is less permeable to larger molecules, such as nitrogen gas.

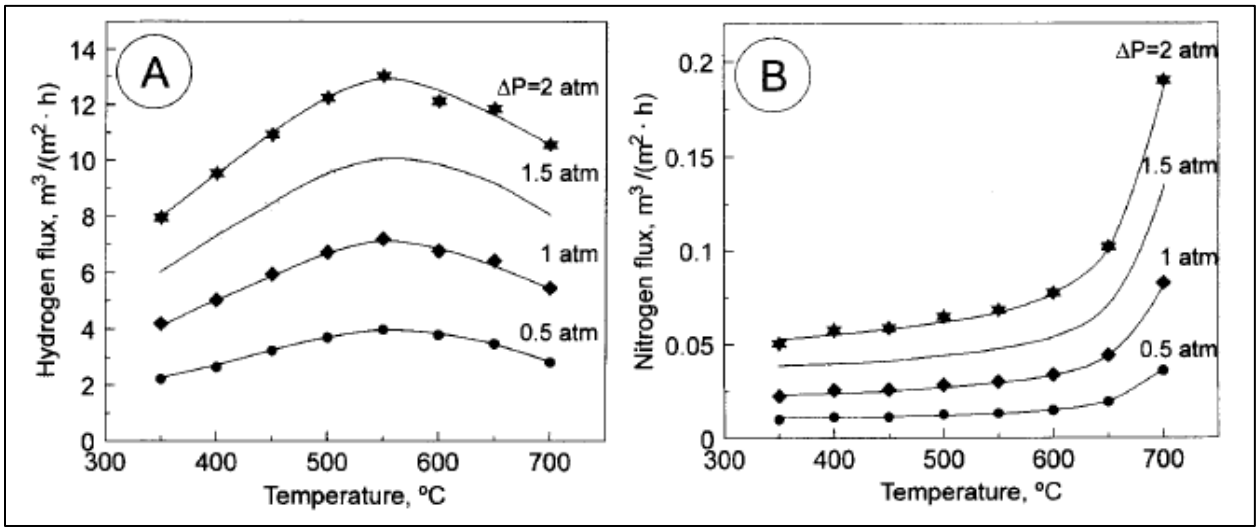

Figure 12: Flux through Pd Membrane for A) Hydrogen and B) Nitrogen (Mardilovich, She, & Ma, 1998)

As the graphs suggest, the membrane operated optimally between 500 and 600 ˚C. The flux of hydrogen through the membrane is more than an order of magnitude higher than the flux of nitrogen.

The presence of other gases besides hydrogen can have a negative impact on the performance of these membranes. As Figure 13 shows, the flux of hydrogen through a Pd/Ag membrane

reduces significantly in the presence of gases such as methanol, water vapor, carbon dioxide, and carbon monoxide. Because of this drop, Pd membranes work best with pure hydrogen.

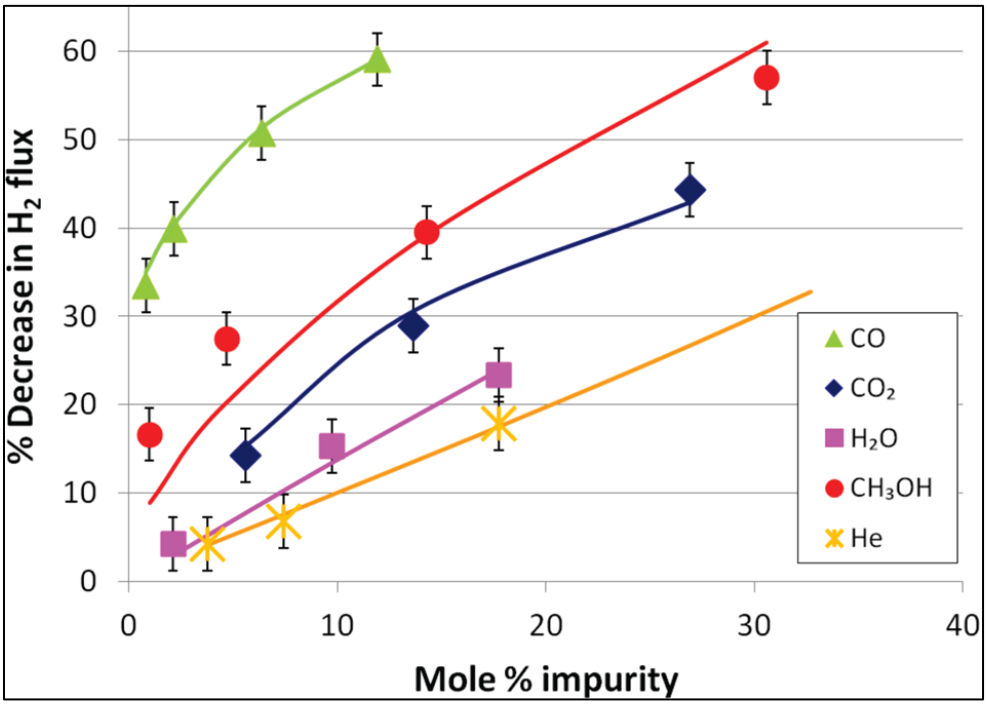

Figure 13: Percent reduction in flux through the membrane based on composition of the feed stream (Sameer H. Israni, 2010)

CO and methanol represent the highest drop in performance of the membrane primarily because of adsorption to the membrane surface. This poisoning of the membrane surface will decrease with increased temperatures, however this decrease is limited. For an increase in temperature from 225 ˚C to 300 ˚C, the decrease in flux ranged from about 5% to about 15% (Sameer H. Israni, 2010). There have been efforts to create methanol reformers that utilize a palladium membrane, however. A catalyst is added to the surface of the membrane, which drives the methanol-steam fuel stream to reform to H_2, CO, and CO_2 in the presence of a heat source. Due to a pressure gradient, the hydrogen moves through the membrane while the other reaction products are rejected and converted to carbon dioxide and water (Yu-Ming Lin, 2000). This creates a pure hydrogen flow, which can then be used as fuel for a PEM or alkaline fuel cell. This ability to reform methanol using the membrane is one that is explored through this MQP project.

Proposed Fuel Cell

What we are attempting to do in this project group is design a fuel cell that integrates all of these components into one compact design. This will be a direct methanol fuel cell with a palladium membrane and an alkaline electrolyte. The methanol-water fuel stream will enter at the anode of the cell and be prevented from passing into the electrolyte by the palladium membrane. The membrane will prevent the poisoning of the potassium hydroxide electrolyte as well as serve as the anode for the cell. Like an alkaline fuel cell, hydroxyl groups move through the electrolyte from the cathode to the anode. Figure 14 shows the relative performances of alkaline, PEM, and direct methanol fuel cells.

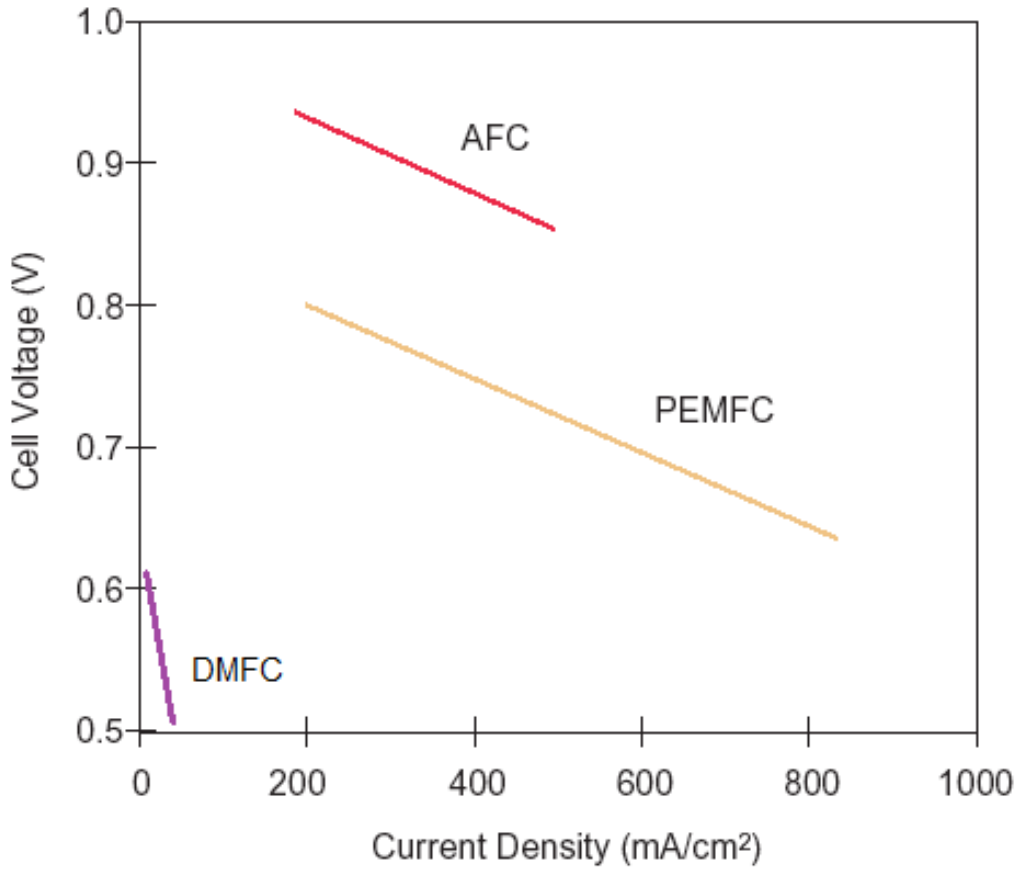

Figure 14: Relative performances between Alkaline, PEM, and Direct Methanol fuel cells

What this chart shows is that direct methanol fuel cells are inferior to the other options in terms of fuel cell performance. The potential benefit of this proposed fuel cell is that it does not require a reformer for the methanol fuel, keeping operating costs low, yet still operates like the

more efficient alkaline fuel cell. The design for our novel cell can be seen in the next section of this report.

3. Design & Methodology

Proposed Cell Design

This fuel cell was designed in a long, tubular orientation meant to stand vertically with an inlet and outlet flow on either side of a circular ceramic which provided support for the electrodes and the electrolyte. Figure 15 shows a basic schematic of the cell, rotated horizontally.

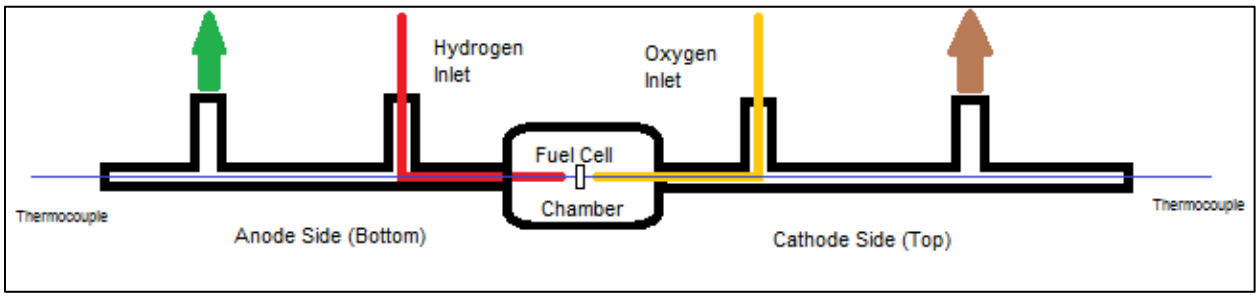

Figure 15: Basic schematic of novel fuel cell design

As the schematic indicates, the true orientation has the anode side pointed downward while the cathode side points upward. H_2 gas, or a methanol-steam mixture, is fed from compressed tanks into the cell via Swagelok 1/16" stainless steel piping. A 1/16"-1/4" adapter was used to connect this feed line to the T-joint that was a part of the main body of the fuel cell. Nuts and ferrules were used to create the air-tight seal. This inlet flow can be seen in the schematic indicated by the red line. The green arrow indicates the outlet for the anode side. Likewise, the yellow line indicates the inlet for oxygen and the brown arrow represents the outlet flow for the cathode side. The blue lines travelling the length of the cell and extending out either end are the thermocouples. They meet the ceramic support in the main fuel cell chamber. A more detailed schematic for this portion of the fuel cell can be seen in Figure 16.

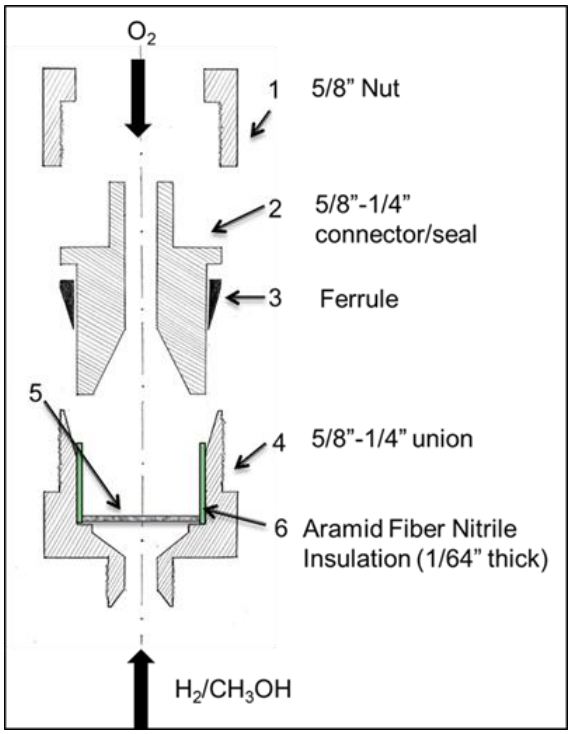

Figure 16: Detailed schematic for the main chamber of our novel cell

This figure also shows the correct vertical orientation, with O_2 coming from above and the hydrogen source coming from below. Arrow 5 in the above diagram indicates where the porous support, gaskets, and NiO layer are located. A close-up view of this section can be seen later in the report in Figure 17.

This novel fuel cell was designed to utilize a planar configuration for the electrodes and electrolyte with a circular silicon carbide (SiC) porous support. These ceramic supports were on average 15 mm in diameter and 2.2-2.4 mm thick. On either side of the SiC chip, gaskets made out of Aramid Fiber Nitrile were placed to help provide air-tight seals to prevent leakage and also help prevent cracking of the chips. On the cathode side of the support, a 1/8" gasket was used and a 1/32" gasket was used on the anode side. On that anode side, after the gasket there was a nickel oxide (NiO) support installed to again provide structural support for the fuel cell. Through this NiO chip there was a small hole drilled to allow for silver wire to come into contact with the anode. This wire connected to the thermocouple which extended outside of the cell and was eventually hooked up to the test station which could monitor electrical output. Back on the cathode side, another silver wire extended down, coming into contact with the cathode.

This was also connected to a thermocouple wire that extended out of the cell to the test station. Around all of the gaskets and support chips, a 1/64” layer of Aramid Fiber Nitrile was wrapped to provide a gas seal and insulation. Figure 17 shows the close-up of the layering within the cell.

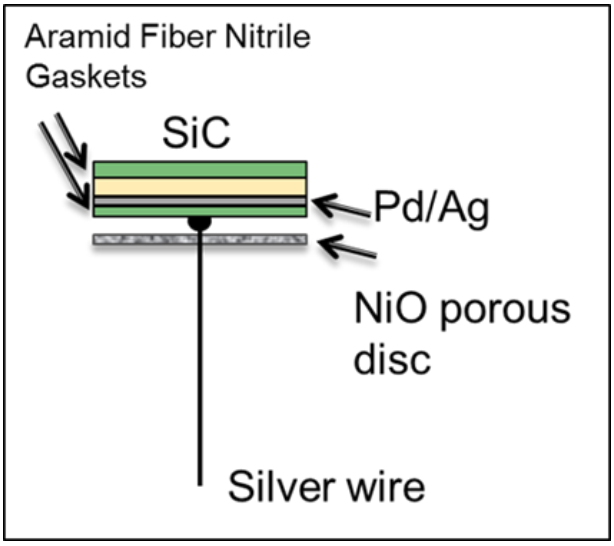

Figure 17: Close-up of the internal setup for the proposed fuel cell design

In this diagram, the tan layer represents the SiC support and the thin, gray layer directly below it represents the Pd/Ag anode. The gaskets were shaped like rings, not whole circles, so that the fuel could come into contact with the electrode surfaces.

The piping used for this experimental fuel cell was Swagelok ¼” stainless steel (SS) piping. This piping was wide enough so that the feed lines and the thermocouples could fit inside, while still having enough room for outlet gases to move to the outlet opening. The inlet and outlet flows were made using Swagelok T-joints, with ¼” attachments that were met with the ¼” piping. In order to create air-tight seals at all of the joints and connections for the fuel cell shell, ¼” SS nuts were tightened around Swagelok ¼” SS ferrules, which had two parts: the front ferrule and the back ferrule. To create a seal around the thermocouple at either end of the cell, a ¼”-1/16” converter was used and met with a 1/16” nut and corresponding ferrule to seal around the thermocouples. The assembled fuel cell can be seen in Figure 18.

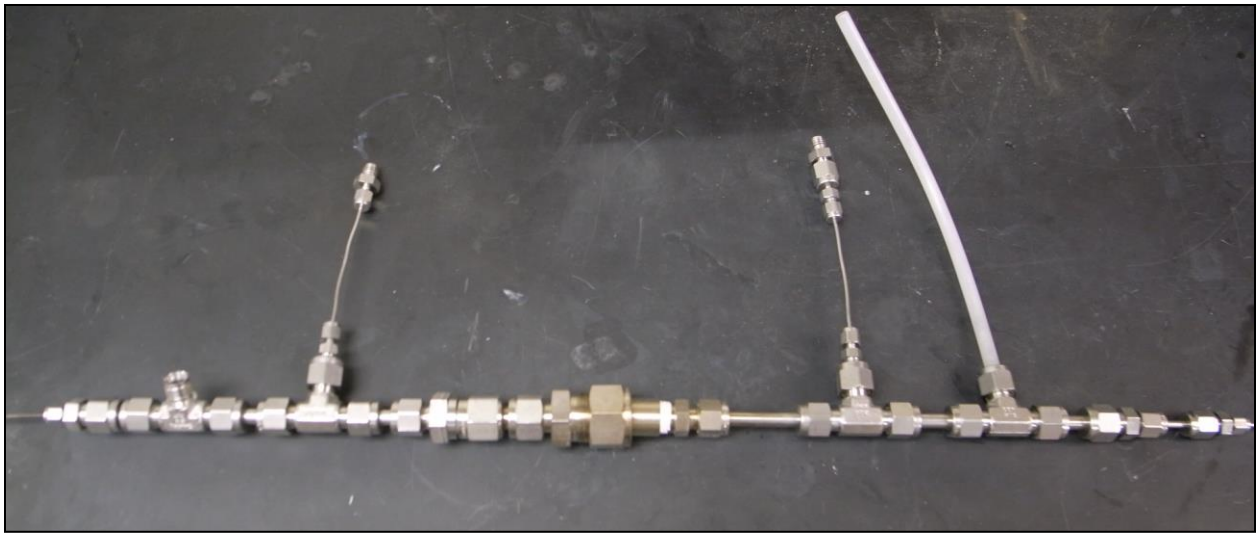

Figure 18: Assembled fuel cell

Electrode Support Preparation

Holding Oven

Before the assembly of the fuel cell could be completed, the ceramic support upon which the cathode and anode would rest needed to be prepared. This porous support, made of silicon carbide (SiC) for these experiments, would also hold the electrolyte for the cell. Throughout the preparation process, there were many steps where the “chips” would need to be dried overnight or just in preparation for another procedure. A holding oven, set to 80 ˚C at all times, was used to dry the ceramic supports.

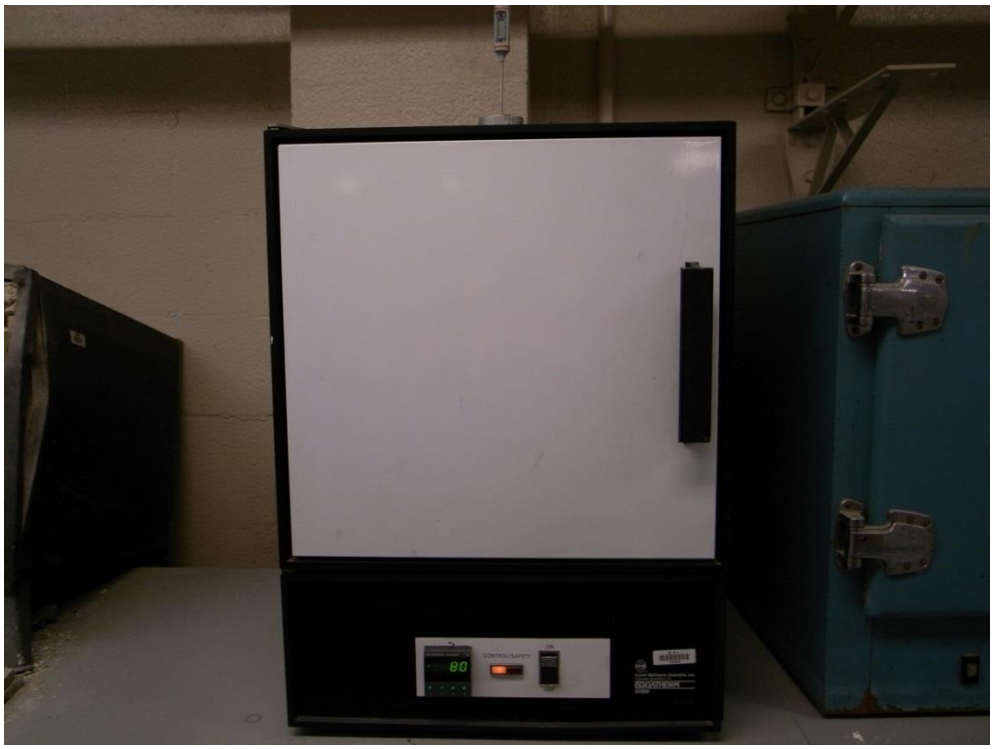

Figure 19: Holding Oven

Electronic Mass Balance

Throughout the course of the project it was also very important to keep track of the mass of each of the SiC chips that were being prepared. All mass measurements were recorded on a Mettler Toledo AG204 electronic mass balance.

Figure 20: Mettler Toledo AG204 Electronic Mass Balance

Electrolyte Absorption Tests

The first step in these experiments was to test the ceramic "chips" to see how much electrolyte, which was potassium hydroxide (KOH), they could soak up while being heated to various temperatures. This test allowed us to determine which temperature would work best later on when it came time to impregnate the support with electrolyte just prior to fuel cell assembly. In order to run this experiment, the ceramic support was placed in a small ceramic crucible and covered in potassium hydroxide pellets so that the entire surface was covered. This crucible was then heated in the oven and held at a constant temperature for 6 hours. This experiment was run at several temperatures, with optimal absorption coming at 200˚C. The heating for this step in the preparation process took place in a ThermoLyne 48000 Furnace, which is shown in Figure 21.

Figure 21: ThermoLyne 48000 Furnace

Activation and Electrode Plating

After the chips were tested to determine the optimal temperature for electrolyte absorption, electroless plating could begin. The process of plating the ceramic supports added the electrodes to either face of the ceramic through a series of plating rounds. Before this could take place, the surfaces of the ceramic needed to be activated. Activation causes palladium nuclei to embed within the pores on the chip's faces. These nuclei would stimulate deposition

of palladium and silver atoms in the subsequent rounds of plating. It required several passes through the activation procedure to achieve the best results.

For the best results, plating occurs at approximately 60 ˚C, so the plating solution would be immersed via a graduated cylinder in a hot water bath while the support was suspended in the solution. This plating setup can be seen in Figure 22.

Figure 22: Plating Process Setup

The cathode side of the support was plated in silver only, while the anode face was plated in both palladium and silver in approximately a 77:23 mass ratio, respectively. Figure 23 shows a support that has been plated with palladium.

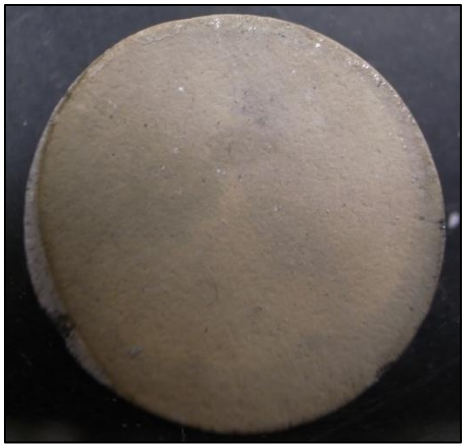

Figure 23: SiC porous support that has been plated with palladium

On the left side of the chip, there is a noticeable line at which the plating stops. This is because the Teflon tape noose that was protecting the edges and opposite face hung over the edge slightly. This is okay because the gaskets that are used later in assembly of the cell cover the edges of the support.

Because of the nature of the plating process, trial and error was necessary to achieve an acceptable ratio and a dense membrane. Our experiments suggest that a 1:1 time ratio for plating palladium and silver would accomplish this goal due to silver's slower plating rate.

An alternative method for activation, called sputtering, was also tested on samples that had undergone regular activation but had had some of their plating peel off during annealing. This was similar to regular activation because it involved the seeding of the chip surface using palladium nuclei. In sputtering, however, these nuclei are shot at the surface in a beam and this process lasted only 30 seconds. This option was used as an alternative after identifying the concerns with peeling.

Figure 24: Sputtering Method Apparatus

Annealing

In order to cause the Ag atoms to diffuse into the palladium layers of the plated surfaces and form an alloy, annealing was required. This created a uniform Pd-Ag membrane across the anode surface of the porous chip. Otherwise, there would be alternating layers of Pd and Ag plated on the surface. This step in the process was accomplished using an annealing oven found in GH 012 lab. The chip was inserted into the metal tube reactor which was then placed into the oven. The exposed ends of the oven were stuffed with fiberglass tape for added insulation. Each chip was annealed at 550 ˚C for 24 hours to cause this migration of silver within the anode plating.

Figure 25: Annealing Oven

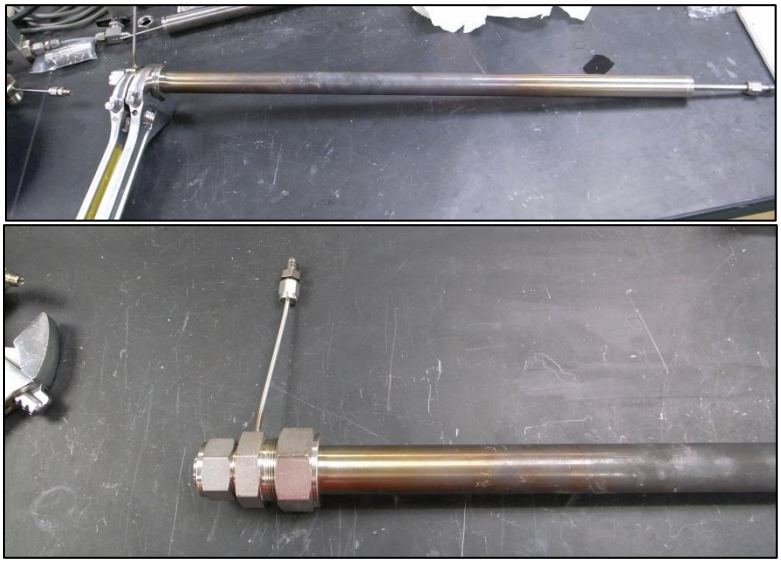

Figure 26: Metal Tube Reactor held in place by wrenches and a closer image of the reactor seal and gas flow hook-up

The reactor allowed for the chip to be in a sealed environment through which helium gas and hydrogen gas could flow at different periods of the annealing stage. When annealing, it is important to monitor gas flow through the reactor. Hydrogen gas should only flow through the reactor at temperatures above 350 ˚C to prevent pollution of the plated surfaces. Helium gas was used at all other times during annealing. These gas flows were monitored using a digital

flow meter which could determine the flow of the gas based on how quickly it could push a liquid bubble through a sensor.

Figure 27: Digital Flow meter

Scanning Electron Microscope & X-Ray Diffraction

After plating and annealing the porous support, it was necessary to analyze the surfaces and make sure that a dense layer had been plated and that the annealing had helped blend the palladium and silver layers into a uniform, Pd-Ag blend. In order to determine that the layer was dense, an Amray 1610 Turbo Scanning Electron Microscope (SEM) with a Princeton Gamma-Tech Avalon EDX light element detector and a RBA-1610 5mc type Robinson Retractable backscattered electron detector was utilized. This microscope scans the surface of a sample by firing a focused beam of electrons at the sample and interpreting the various signals that are emitted by their interaction with the surface. Using this technology, a magnified image of the surface and basic elemental information were ascertained. The goal when using the SEM was to find no pinholes and have no detection of silicon in the elemental analysis, indicating the chip had been completely covered by the plating.

Figure 28: Scanning Electron Microscope (SEM)

Figure 29: SEM Analysis Computer

Once it has been determined that the membrane was dense and no pinholes were detected, the plating could be analyzed to see whether annealing had properly caused the silver to diffuse into the palladium layers, creating a crystalline alloy. This was done with a Rigaku Geigerflex X-Ray Diffractometer (XRD) equipped with a CuKα radiation and curved crystal monochromator. The XRD works by firing x-rays at the sample surface at a variety of angles, or thetas (θ), and then interprets the corresponding signals given off by the sample to determine molecular information about it. For this analysis, we were looking for the sample to give off a distinct Pd-Ag signal, indicating an alloy as opposed to two separate signals: one for unmixed palladium and one for silver.

Figure 30: X-Ray Diffractometer

Preparing Gaskets and Nickel Oxide Supports

Once the ceramic supports had been prepared, additional components of the cell needed to be prepared. One was the NiO chip that would be placed under the SiC chip to offer additional support. In order to prepare these, a hole was drilled in a piece of nickel metal. This nickel

would serve as the nickel oxide support and the hole allowed for the silver wire to extend from the thermal couple and attach to the porous support. This nickel was then polished using a belt sander to make it the correct shape to fit into our cell. Once it had been polished to the correct dimensions, it was oxidized in an oven at 900˚C for 12 hours, forming a harder nickel oxide.

Two types of gasket were also prepared for our cell design. Both were made out of Aramid Fiber Nitrile, one being 1/8" thick while the other one was only 1/32" thick. These were made by boring out the center hole using a hand hole cutter and then polishing the outer surface until it too fit inside the metal fixture. It was important when preparing these components that they fit snug inside the cell so they needed to be very carefully polished. These components of the cell can be seen in Figure 31.

Figure 31: The Two Gaskets (top-right), the NiO Support (bottom-left), and the Hand Cutter Used to Make the Gaskets (center)

Setting up a Test Run

Once the two halves of the cell were tightened and the moving parts were fixed in place, it was time to connect the cell with the test station. The test station could measure the voltage across our thermocouple wires as well as plot graphs of voltage over time, current over time, voltage vs. current, etc. First, the bottom half, or the anode half, was fixed next to the test station using a G-clamp attached to the table and claw clamps extending off of that. A stabilizing rod would act as the backbone of the fixture. The bottom half was fixed into place using the clamps,

making sure that the feed lines could be hooked up correctly without bending the tubing. Next the NiO support, the gaskets, and the SiC porous support were inserted into the top of the anode half. It was necessary to make sure that the anode face actually was facing downward, or else the experiment would not run properly. Next, the top (cathode) half of the cell was attached and the 5/8” connector nut was gently tightened, so as not to break the chip. Once this half was secured using the clamps, the feed lines were connected and the anode and cathode senses on the test station were connected to the corresponding thermocouples. The heating rods and a third thermocouple were tied around the central chamber using fiberglass tape and then we proceeded to wrap the whole cell in more fiberglass tape. This helped keep the heat in throughout the tests. Figure 32 and Figure 33 show the fuel cell wrapped up and hooked up to the testing station.

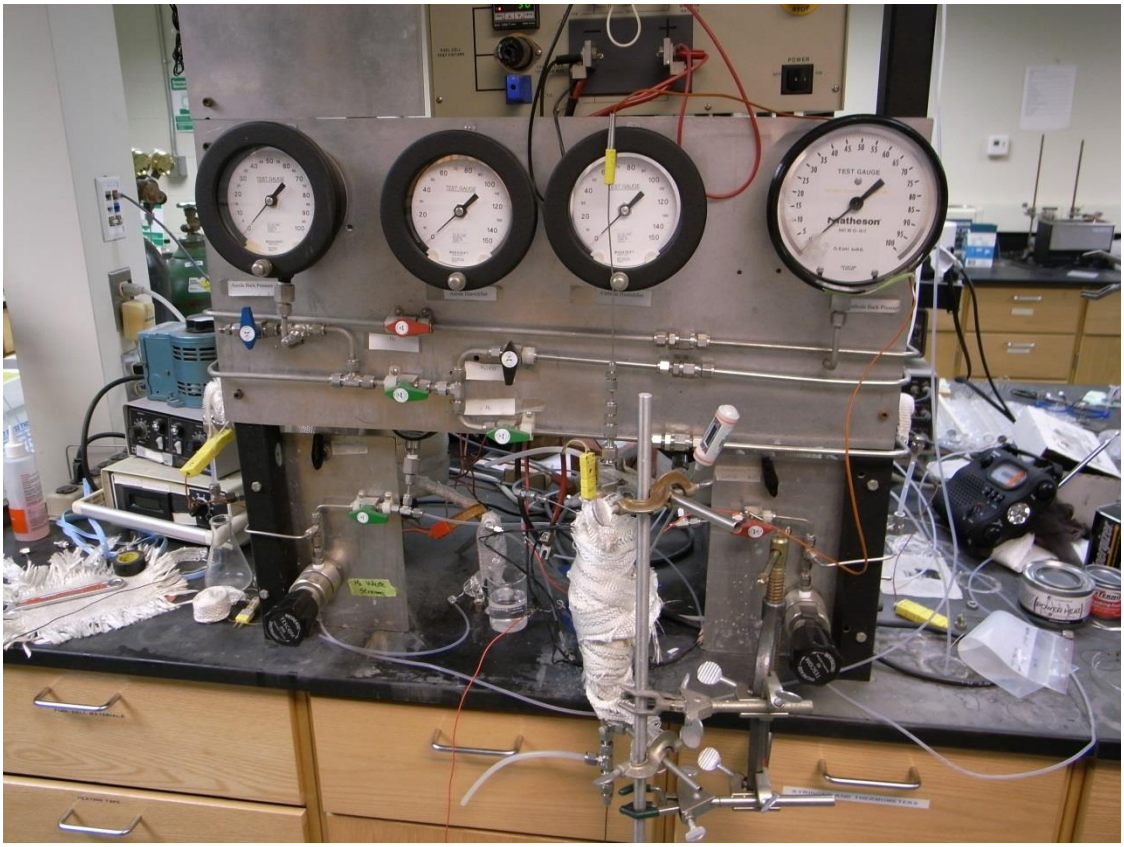

Figure 32: Fuel cell set up next to the testing station

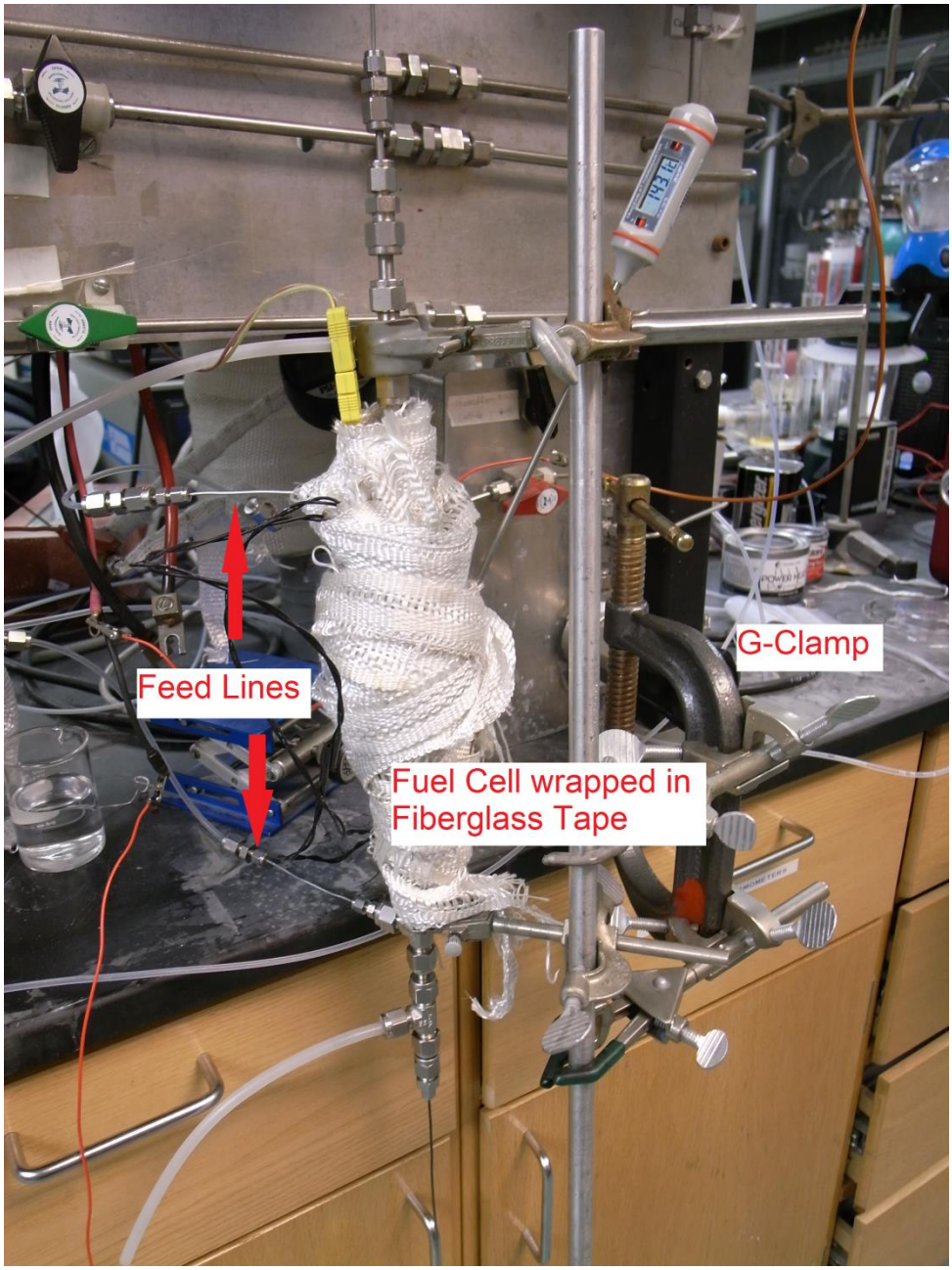

Figure 33: Closer view of the fuel cell set up next to the test station

Once the fuel cell was in place and hooked up properly to the testing station, the heating rods were set to 200 ˚C and the system was given time to heat. Meanwhile, nitrogen gas was purged through the system. By only having nitrogen flow through each side of the cell one at a time, we were able to verify that there were no leaks in our setup and nothing was crossing through the cell to the other side of the porous support. Once the system was purged, the hydrogen and

oxygen feeds were applied and the experiment could begin. The test station controls could be operated via a computer in the lab.

Preparation Step-By-Step Procedures

KOH Impregnating

1. The ceramic chip was allowed to soak overnight in a beaker of water to remove any potential contaminants.
2. This chip was then placed in a petri dish and left in an oven overnight to dry at 80˚C.
3. The chip was removed from the oven and allowed approximately 10 minutes to cool.
4. This sample was then weighed to get an initial measurement.
5. The chip was placed into a ceramic gooch crucible and covered with ≥85% Potassium Hydroxide, KOH, pellets.
    a. It was important to make sure that the pellets completely covered the surface of the ceramic chip but that as little KOH was used as possible.
6. The crucible containing the ceramic support and the KOH pellets was placed into a ThermoLyne 48000 Furnace.
7. The ‘PAR’ button on the furnace was pressed as many times as necessary until ‘r1’ appeared on the keypad. 10.00 was entered for this setting using the up and down arrow keys to change the number.
8. The ‘PAR’ button was again pressed as many times as necessary until ‘L1’ appeared on the menu screen. This controlled the temperature at which the furnace would hold to allow the KOH to melt and soak into the pores of the ceramic chip. Three tests were run, with the temperature set to 200˚C, 250˚C, and 300˚C, respectively.
9. The ‘PAR’ button was again pressed until ‘d1’ appeared on the menu. This set the amount of time that the oven would hold at the desired temperature. This was set to 360 (in minutes = 6 hours).
10. Whenever it was necessary to change menus from this point forward, the ‘PAR’ button was used to switch from one to another.

11. The ‘r2’ menu was set to 1.00. This was the ramp-down rate (in ˚C/min) for the temperature after the six hours of holding at the desired temperature was completed.
12. The ‘L2’ menu was set to 180. This was the temperature (˚C) at which the oven held until the sample was removed and the run was terminated.
13. Made sure that ‘d2’ was set to 9999. This was the duration that the oven would hold at 180 ˚C. This was to prevent the oven from shutting off and allowing the KOH to re-crystallize before the sample could be removed.
14. The ‘PAR’ button was then hit repeatedly until ‘prog IdLE’ appeared on the screen. While this was still on the screen, the up arrow key was hit so that the screen now said ‘prog run’. This started the program.
15. After six hours was completed, furnace was set back to ‘prog IdLE’ by hitting the down arrow key while on the ‘prog’ menu and the crucible was removed.
16. The ceramic chip was removed from the crucible and the surface of the chip was gently wiped with a moist paper towel to remove any crystallized KOH on the surface and then the sample was weighed on a balance. Fill the crucible with water and allow it to soak to dissolve any crystallized KOH.
17. The change in mass was calculated using the initial mass reading to find the mass of the potassium hydroxide soaked up. By dividing this value by the original mass of the porous support, % uptake was also calculated.
18. The chip was placed in a beaker of water to dissolve the KOH which it had soaked up during the test. The water was changed frequently to maintain a high concentration gradient and pull the KOH out of the ceramic chip faster.
19. The procedure was repeated twice more at different oven temperatures and the % uptake of KOH was compared to find the optimum temperature.

Pd Activation – Pd Seeding

1. The ceramic chip was first soaked in a beaker of water for several hours to remove potential contaminants and then left in the oven overnight at 80˚C to dry.

2. After removing the ceramic chip from the oven, it was “noosed” with Teflon tape. This means that the chip was wrapped up by Teflon tape in the shape of a noose in order to allow for the chip to be suspended in the activation solutions. To do this:
    a. A stretch of Teflon tape approximately 18 inches in length was laid flat along the surface of the table, with the chip held, by tweezers, on edge in the middle of this piece.
    b. The tape was then folded in half so that the two severed ends were touching, thus wrapping the ceramic chip up at the opposite end where the fold occurred.
    c. It was made sure that the chip remained on end and that the two circular faces of the chip faced perpendicular to the length of the tape.
    d. The excess tape which wasn’t in direct contact with the ceramic chip was pinched off at the chip in a way that covered the entire narrow edge.
    e. The tape that was not touching the chip was twisted so that it was securely around the chip. This would be the rope from which the sample could hang into each solution during the activation process.
    f. Excess tape that was covering the two circular surfaces of the chip was peeled back so that only the thing edge was covered by Teflon tape.
    g. In summation, the chip had Teflon tape wrapped around the entirety of its circumference while none covered either face. There also was a twisted “rope” from which the chip could hang to suspend it in the activation solution.
    h. The rope was tied to a metal support which could then rest across the opening of the graduated cylinder and allow the ceramic to dip into the solution.

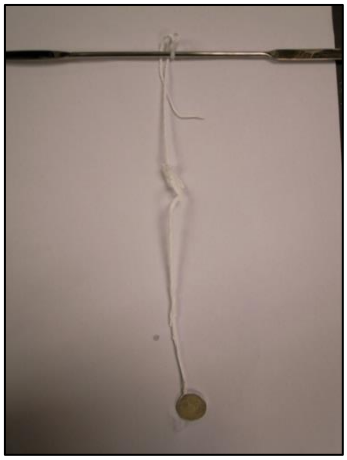

Figure 34: Noosed Ceramic Chip Setup

Figure 35: Closeup of Noosed Chip

3. The chip was immersed in water to wet the surface while the activation solutions were prepared.

Activation Solution Preparation

1. Two 100-mL graduated cylinders were filled with approximately 100 mL of DI water.
2. Two 50-mL graduated cylinders were filled with approximately 20 mL of DI water.
    a. In one of the 50-mL graduated cylinders, 0.05 mL of HCl was added using a pipette. Then DI water was added to the cylinder until there was a total of 50 milliliters of liquid in the cylinder. This was the HCl solution in the activation process.
    b. In the other 50-mL graduated cylinder, again 0.05 mL of HCl was added using a pipette. The cylinder was filled until the total volume of liquid reached the 50 mL mark again. Then 0.05 g of solid $SnCl_2$ was massed out and added to the solution. An electronic balance was used to mass out the tin chloride to ensure the proper amount was used. Persistent stirring was needed to make the solid dissolve in the solution.
3. In a third 50-mL graduated cylinder a pre-mixed solution of $PdCl_2$, found in the Center for Inorganic Membrane Studies, was added, again filling the cylinder to the 50 mL mark. This solution came from a mixture with the following component ratios:
    a. 1 L H_2O : 0.1 g $PdCl_2$: 1 mL HCl

Activation Process

1. The five prepared graduated cylinders were arranged into the following order: $SnCl_2$ mix, DI water, $PdCl_2$ mix, HCl mix, DI water. Below is a diagram of the activation setup:

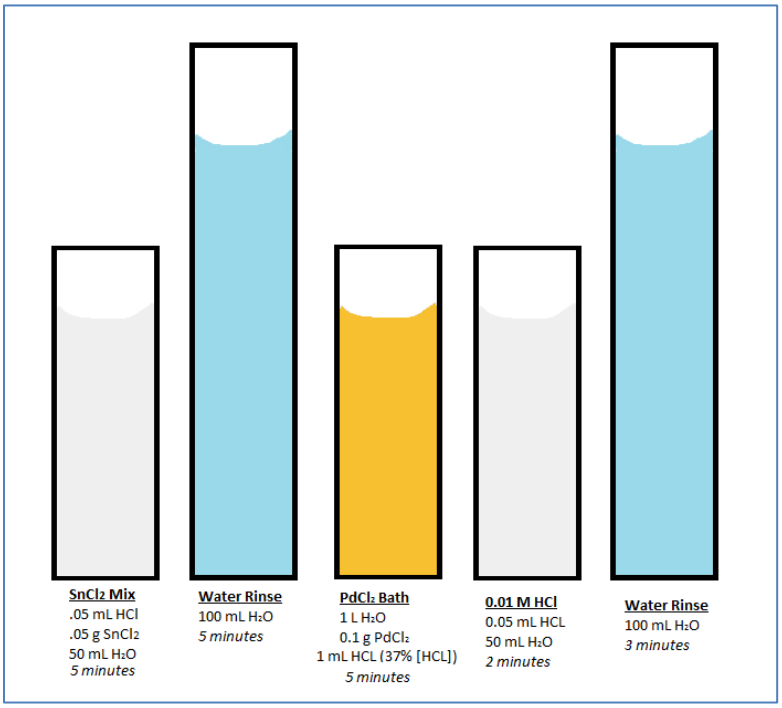

Figure 36: Activation Process Setup Diagram

2. To begin activation, the noosed chip would begin by being suspended in the $SnCl_2$ mix cylinder for duration of five minutes.
3. After five minutes, the chip was moved into the first DI water cylinder, where it remained for five more minutes.
4. After five minutes in the water, the chip was removed from the water and inserted into the $PdCl_2$ solution for five minutes as well.
5. From there it was moved to the HCl mixture where it only spent 2 minutes, and then finished in the final DI water graduated cylinder for three minutes.
6. This encompassed one pass through the activation procedure.
7. For optimal activation and seeding, several passes were needed for each chip. The procedure was repeated multiple times for a total of six passes.
    a. With each pass lasting a total of 20 minutes, this made the total activation process last 2 hours.

Palladium Plating Procedure

1. A clean 50-mL graduated cylinder was rinsed with DI water and then filled with 10 mL's of pre-prepared Pd Plating Solution per each chip that was being plated. *(Ex: If two chips are being plated, then 20 mL of solution is used)*
    a. This plating solution was taken from the Center for Inorganic Membrane Studies.
2. Using a 1-mL syringe, 0.06 mL of Hydrazine, N_2H_4, is added to the solution per chip being plated. *(Ex: 0.12 mL was used for 2 chips)* This served as the reducing agent for the plating reaction.
3. Parafilm was used to cover the opening of the graduated cylinder and then it was transported downstairs to the lab.
4. Using a hot plate, a water bath was heated to between 55-60 ˚C with the 50-mL graduated cylinder of solution in the water bath.
    a. While this was heating, the chips were prepared. Using Teflon tape, the chips were noosed, as explained in the activation procedure, to allow for them to be hung from a support into the solution. The difference this time from the preparation of the activation process was that it was made sure that the tape fully covered the edges AND back-side of the chip so that they were not exposed to the plating solution.
    b. The ends of the tape ropes were tied to a thin metal rod which would rest across the opening of the graduated cylinder.
5. Once the solution was at the required temperature, the chips were lowered into the solution and the timer was started. Periodically, the temperature was checked to make sure that it was within an acceptable range.
    a. It was necessary to make sure that the ropes were the correct height to make sure the chips were suspended in the solution without resting on the bottom of the graduated cylinder.
6. After allowing the chips to plate for the desired amount of time, they were removed and transferred into a graduated cylinder filled with DI water. This was necessary to remove

any ammonia which might have been on the surface of the SiC chip. This graduated cylinder was placed into the water bath.

7. The water in the graduated cylinder was changed after about fifteen minutes and the chip was allowed to soak in fresh water for approximately another 15 minutes before the noose was removed. The chip was placed in a petri dish and returned to the 80 ˚C oven to dry.
8. To dispose of the plating solution, it was brought to the top floor of Goddard Lab into the Center for Inorganic Membrane Studies Lab. Here, it was dumped into a chemical waste barrel.
9. After dumping the solution, the graduated cylinder was rinsed with DI water and then filled with 30 mL's of Aqua Regia (nitro-hydrochloric acid). It was covered using Parafilm and left in a chemical hood to allow time for cleaning.

Silver Plating Procedure

1. This procedure was the same, in principle, as that for the Pd Plating. The differences were:
    a. 10mL of Ag Plating Solution per chip was used instead of the Pd Plating Solution.
    b. 0.07 mL of Hydrazine was added to the solution per every 10 mL of Ag Plating solution used.
    c. For each chip, a thin, non-dense layer of Ag was needed on the back-side. Therefore, it made sense to plate this layer while also plating the other side. When plating both sides simultaneously, obviously neither side was covered with Teflon Tape. The edges of the chip still needed to be covered, however.

Annealing Process

1. The ceramic chip was inserted into a glass tube, approximately 12 inches long, used to inject the chip into the metal tube reactor.
2. By comparing the lengths of the glass tube and the reactor shell side by side, a marking was made on the outside of the metal shell to show where exactly the chip should have been once inside the reactor.

3. Fixture was closed and tightened using wrenches.
4. The reactor was placed into the annealing oven. Using the mark made earlier showing where inside the reactor the chip should lie, the chip was lined up with the epicenter of the oven. This made sure that it would reach the desired temperature.
5. Fiberglass tape was wrapped around either end of the reactor shell once in the oven to mitigate heat loss.
6. The top of the oven was closed and the metal hoses to which the gas supply was attached were connected to either end of the reactor.
7. The machine was turned on and then the Setting button was held until the menu changed.
8. The Setting button was pressed repeatedly until the program menu was reached. For this option, 1 was entered using the up and down arrow keys.
9. *In order to change menus, the Setting button was hit each time.*
10. At the 'SSP' menu, the value 20 was entered. This was the Set Starting Point for the temperature and the value was set at room temperature.
11. The 'Stc' menu was ignored.
12. For the 'SP1' menu, the value 550 was entered. This was the temperature to which the machine would rise initially, in degrees Celsius.
13. At the 'tm1' menu, 4.25 was entered. This was the duration of the ramp-up period (hours.minutes). This was calculated knowing that the typical ramp-up rate was 2 degrees Celsius per minute.
14. 'SP2' was the temperature at which the machine would hold throughout the duration of the annealing process. It was set to 550 again.
15. 'tm2' was the Duration of the holding stage. It was set for 24.0, which was in hours.
16. 'SP3' was the temperature that the oven would be brought to once the 24 hour annealing step was complete. It was set to 20 as well.
17. The ramp-down rate for this cooling was set to be the same as the ramp-up rate for the desired process, 4.25.
18. 'SP4' was ignored.

19. ‘tm4’ was set as ‘off’, which is why ‘SP4’ was able to be ignored.
20. The Setting button was hit repeatedly until the ‘SSP’ menu was reached once again. The Setting button was pressed and held until the original temperature menu was back on the screen.
21. It was important to make sure that the helium tank supplying this apparatus was full. The On/Off Valve within the glass work area that is marked with a white ‘He’ tag was opened. Before opening the helium tank, it was important to make sure the On/Off valve controlling the flow next to the gas tanks was correctly pointed in the direction for the pure helium flow and NOT the hydrogen-helium mix. The helium tank was opened.
22. The green knob inside the work station and the metal needle valve along the helium flow line were used to adjust the gas flow. The flow was adjusted until the small pressure reader located just outside of the glass work area read approximately 2-3 psig and the digital flowmeter found within the glass hood indicated a gas flow of approximately 5-10 mL/min.
23. The Setting/Run button was held until a click was heard. This signified that the heater had turned on.
24. Once the temperature reached 350˚C, the helium gas flow was shut off and the hydrogen gas flow was turned on using the On/Off valves found in the glass work area. Like the helium flow, the tank in the lab corner was checked to ensure that gas was available and the valve was then opened. This line was also labeled with a white tag, but this tag read “H_2”.
25. The gas flow was adjusted until once again the pressure reader indicated 2-3 psig and the digital flowmeter read between 6-10 mL/min. Adjustments were made as necessary to the flow of the hydrogen gas using the green knob which was along the gas line.

XRD Surface Scanning

1. The X-Ray Diffractometer was turned on by flipping the 5 startup switches in ascending order. They were all numbered from one to five. There were several rules to follow when turning on these switches:
    a. Switch 1 should have been on already. It is permanently left on.

   b. For Switch 3, which turned on the cooling unit, the valves for the cooling water feed and exit needed to be opened first. These were the two yellow On/Off valve handles along the copper piping on either side of the water filter. Once this line was opened, the cooling unit was flipped on.
   c. Power switches 4 and 5 were only turned on once the sample was loaded into the Diffractometer.
2. To load the sample:
   a. The hand-screw located on the circular cap of the sample chamber's side was removed. This allowed the cap to come off and expose the sample chamber.
   b. The sample was placed into the well of a plastic, rectangular filter load disk. It was important that the depth of the filter disk well was such that the ceramic chip's surface was level with that of the rest of the plastic disk.
   c. The loaded plastic disk was inserted into the chamber by sliding it on top of the two prongs within the chamber which held the sample in place.
   d. The cap was replaced on the chamber and the screw was tightened.
3. The glass doors on the case of the XRD were closed so that the left-most door was flush with the edge and the white rectangle on the middle door was directly over the red dot on the case's frame. The machine would not turn on otherwise.
4. Switches 4 and 5 were flipped on and the voltage and current knobs were set to 37.5 and 25, respectively.
5. To run the test and analyze the data:
   a. MDI DataScan4 was opened on the computer closest to the machine (the left computer).
   b. First a calibration test was run on the quartz sample found in the hood with the XRD. To do this select 'Control' and then 'MDI Databox'. In the MDI Databox menu, click on the 'Function' tab and then 'Scan Line' below that. It should already have been set to quartz so then the sample was scanned.

        i. After the run was complete, the system told us how far off the standard line it was and asked if we would like to adjust the goniometer accordingly. We said 'OK'.
    c. Switches 5 and 4 were turned off, the quartz sample was removed, and our sample was loaded into the diffractometer.
    d. Under the 'Scan' tab, 'Scan this range' was selected.
    e. The low and high angles for the scan were set to 10 and 90, respectively. This range corresponded with the values of 2θ, which was the angle at which the X-rays would hit the sample.
        i. This range can be reduced once the operator is familiar with the samples they are analyzing and know where the distinct peaks in the reading will show up.
    f. The step size was changed to determine how many degrees the beam angle varied in between readings. This was typically set to 0.02-0.05. A larger step size meant that the test would take less time but would not be as precise a reading.
    g. The data was saved using a name that would indicate which chip was analyzed, which side of the chip, the date, and whether or not that test was pre- or post-annealing.
6. The file needed to be saved onto a flash drive and transferred over to the right computer. To analyze the results, login and open *MDI Jade 8*.
7. 'File' was selected, and then 'Read' to open the MDI file. It was opened once it was located. The XRD pattern would then be visible on the large window.
8. The BG function was used to remove the noise background
9. Identify→Search/Match Setup created a Phase ID window, which popped up into the foreground.
10. Based on the elements expected in the result, a filter could be used. All Subfiles was selected in the left window, while Use Chemistry Filter was selected in the right window. This brought you to a periodic table where one could select the elements they were looking to see if the sample contained. Our runs involved Pd, Ag, and Si.

11. Click the S-M button in the top right corner of the Phase ID window. Figure 37 below shows the correct selections.

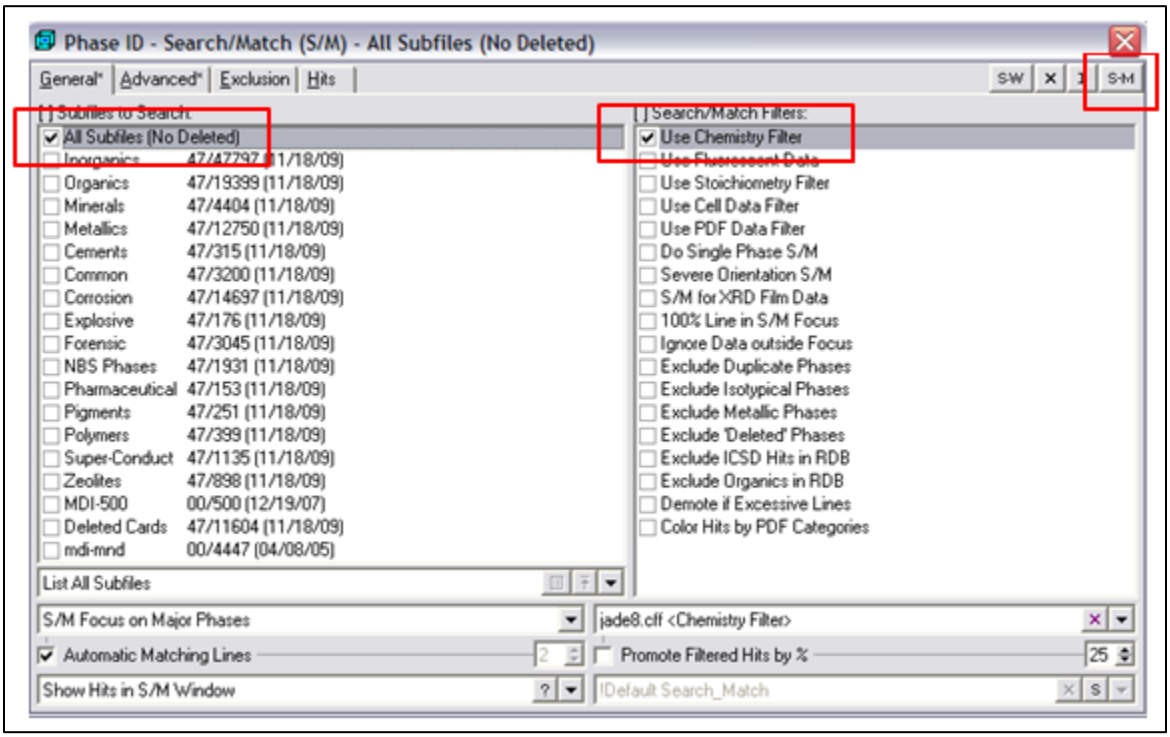

Figure 37: Window view showing the correct selections for the XRD analysis

The window closed and the original plot returned to the forefront. Below it, there were several options for the elements that were selected from the table. By clicking the check-box next to each option, the program would show where the relevant peaks were for each type of each element and one could use the information to determine which elements comprised the sample.

12. The chemicals that accurately matched the peaks from the sample were left checked. This left a small bar below the main plot showing where each checked element's peaks were. These marked peaks should have matched up with those from the graph.
13. File→Print Setup was selected, where there were several options for how to display the data. The option showing the original plot with the locations of the peaks for each element selected was chosen, and then the file was saved as a jpeg file.

14. Additionally, If one wanted to compare multiple samples, the file should be saved as *.txt so you can reopen the file in Excel, and then a graph of multiple data could be generated. For this, one should go to File→Save→Primary Pattern as *.txt.

Setting up an Experiment

1. A G-clamp was fixed to the table on which the testing station sits. Off of this G-clamp arm claw clamps were used to hold a metal rod approximately 24" long. This was the backbone of the support structure for our fuel cell.
2. Additional claws were attached off of the metal rod to hold onto the fuel cell. It was important that these claws be positioned correctly so that they did not interfere with the region of the cell that was to be heated and also so that the cell was at the correct height to attach the fuel feed lines.
3. The bottom-half of the constructed cell was placed into the bottom claw clamp, making sure that it was perpendicular to the table surface. Again, it was necessary to make sure that the feed lines were able to be connected.
4. One of the 1/32" gaskets was inserted into the fuel cell chamber and then the nickel oxide support was placed on top of it. It was necessary to make sure that the silver wire attached to the thermal couple was protruding from the drilled hole at the support's center.
5. An additional 1/32" gasket was placed on top of the NiO chip. Then a thin wrap of insulation was inserted into the chamber so that it wrapped around the walls. This helped seal the fuel cell while also preventing short-circuiting from contact with the walls.
6. Next, the SiC support was inserted into the chamber. It was important to make sure that the side with both Pd and Ag, the anode, faces downward.
7. Lastly, the 1/8" gasket was inserted and the chamber was sealed by attaching the top half of the cell. It is important not to over-tighten the chamber to avoid cracking of the support.
8. The top claw was tightened to secure the cell in position and make sure that it was not being bent or tilted.

9. The fuel feed lines were hooked up to the appropriate attachments on the fuel cell. The fuel, in this case H_2 or methanol, was hooked up to flow to the anode side of the cell while the oxygen flowed to the top.
10. The wires from the 'Anode Sense' and 'Cathode Sense' on the test station were attached to the corresponding thermal couples on our fuel cell using alligator clamps.
11. The heating rods were placed on either side of the fuel cell main chamber along with another thermal couple to measure the temperature of the experiment. These components were tied to the cell using fiberglass tape. More fiberglass tape was used to completely wrap the cell to add insulation.
12. Once the cell was ready for testing, the control computer was turned on and the 'FuelCell' program was opened from the desktop. The test station was also turned on.
13. Under the Setup Cell control box, the surface area and number of stacks were entered.
14. Under the Setup Fuel box, the desired Minimum Flow Rates for the fuel feeds to each electrode were entered. This was to be the feed flow for the experiment. Then the Load Based Flow was set to the same value as the fuel flows.
15. Next, both fuel lines were connected to a nitrogen gas tank and the system was purged with N_2. During purging the system was checked for leaks around the seal of the main chamber and crossover through the silicon carbide chip.
16. The anode feed line was connected to the hydrogen gas tank and the cathode line was connected to the oxygen tank.
17. The fuel cell thermal control box on the test station was set to the desired temperature, initially 150 ˚C, beginning heating. The temperature was slowly raised up to 250 ˚C if no voltage was achieved at the lower temperatures.
18. Next to the 'Setup Experiments' box in the FuelCell interface, the 'New' button was selected. Under this new tab, the type of experiment that was going to be run was selected. For the first run, an Open Circuit experiment was run. The duration of the experiment was set for 5 hours.
19. The fuel flow was turned on by clicking the 'Apply Fuel' button in the top-left corner of the screen.

20. Next, ‘Run Sel.’ was clicked, starting the recording for the experiment.
21. Under the ‘Graphs’ tab at the top of the window, select ‘vs. Time, then ‘E_Stack (V). This would give a plot of the voltage vs. time for an Open current. This was the first plot generated for our testing.
22. Once the experiment ran through, the file was saved and the test station was allowed to cool down. The SiC chip was removed from the chamber, enclosed between two petri dishes, and placed back in the holding oven.

4. Results

Potassium Hydroxide Loading

Prior to testing the cell, preliminary tests were run to determine the best temperature to heat the KOH to as well as the optimum duration. By calculating the volume of the porous supports, we were able to take the density of silicon carbide and calculate how much empty space there was within each chip, in other words calculating the total volume of pores for each support. Then, by measuring the weight of electrolyte that was loaded into the support for each test, we could calculate the volume of electrolyte absorbed. By comparing these two values we were able to estimate the percent of the pore space that was filled by electrolyte and determine which conditions yielded the highest result. Three temperatures, 200 ˚C, 250 ˚C, and 300 ˚C were tested initially. Next, we tested three different lengths of time, 3 hours, 6 hours, and 24 hours, to see which gave the highest result. Table 1 and Table 2 show the testing data.

Table 1: Dimensional and compositional data for the ceramic supports

Initial Data	Mass	Thickness	Diameter	Volume	Density SiC	Porosity, ϕ	Pore Volume
Units	*(grams)*	*(mm)*	*(mm)*	*(cm^3)*	*(g/cm^3)*	-	*(cm^3)*
Chip 1	0.6799	2.216	14.99	0.3911	3.21	0.4584	0.1793
Chip X	0.6958	2.23	15.2	0.4047	3.21	0.4643	0.1879
Chip 2	0.6829	2.246	15	0.3969	3.21	0.4640	0.1842

Table 2: Electrolyte load test results

KOH Tests	Initial Mass	Max Temp	Duration	Final Mass	Uptake	Density (KOH)	Volume (KOH)	% Pores Filled
Units	*(grams)*	*(Celsius)*	*(hr : min)*	*(grams)*	*(grams)*	*(g/cm^3)*	*(cm^3)*	*(%)*
Chip 1	0.6799	200	6:00	0.9658	0.2859	2.04	0.1401	78.18%
Chip 1	0.6793	250	6:00	0.877	0.1977	2.04	0.0969	54.06%
Chip 2	0.6269	300	6:00	0.8243	0.1974	2.04	0.0968	52.54%
Chip 2	0.6351	200	3:00	0.9589	0.3238	2.04	0.1587	86.19%
Chip 2	0.6349	200	6:00	0.9742	0.3393	2.04	0.1663	90.32%
Chip X	0.7169	200	24:00	-	-	2.04	-	N/A

As the data indicates, a significantly higher uptake was measured for the 200 ˚C run than those at the higher temperatures. The data is so convincing that we could confidently say that this

would be the desirable temperature. The reason that we could not go to a lower temperature was because the potassium hydroxide chips that we were using melted at 180 ˚C.

After determining that 200 ˚C would be the best temperature at which to load the electrolyte, we ran more tests comparing the uptake for various test durations. As that data also shows, between three and six hours is a good range for electrolyte loading. The test for 24 hours did not register any results because the KOH actually reacted with carbon dioxide in the air while sitting in the oven and formed potassium carbonate, a crystal or soft white powder. An image of the sample after being removed from the oven is shown in Figure 38.

Figure 38: SiC chip covered in potassium carbonate crystals

Not only did this mean that most, if not all, of the electrolyte did not end up inside the support, but because of this reaction, the chip was actually stuck to the crucible in which it sat and was ruined while trying to remove it. The Pd/Ag membrane was stuck to the bottom and most of it was ripped off when the chip was taken out.

Figure 39: SiC chip with some of its plating ripped off

The lighter spots on the surface of this chip are where the plating was ripped off of the chip altogether. Obviously this is an unwanted occurrence and the 24 hour electrolyte loading was deemed unsuccessful and an unviable option. For both the three- and six-hour tests, the electrolyte melted as desired, did not react with the atmosphere, and measurements indicated that both saw high levels of success with KOH absorbance.

One interesting occurrence during testing was the addition of solid electrolyte into the reaction chamber. By adding solid KOH and a drop of water, then closing the chamber and allowing the KOH to melt as the test heated up, we saw much greater results, almost seven times as high as previous attempts. This might have helped because it counteracted the leaching of electrolyte out of the porous support and the drop of water may have helped to liquefy the electrolyte, allowing for ion passage.

Electrode Plating

The lengthiest portion of fuel cell fabrication was the plating of palladium and silver. This process required several rounds of plating in solution to deposit enough on the support faces to get a dense Pd/Ag alloy for the anode and a silver layer as the cathode.

There were several obstacles encountered during the plating process of this project. One issue was the method of activation. When it came time to anneal our supports to create our Pd/Ag alloy membrane, we found that the plating would peel or flake off of the SiC chip. Figure 40 show the effects of peeling and flaking after annealing.

Figure 40: a) and b) Peeling-off plating due to annealing

We hypothesized that this was occurring because the nuclei that were being seeded during activation were larger than the pores of the porous support. This would cause them to be deposited on top of the surface like a carpet as opposed to being rooted within the pores and providing mechanical strength which would hold the palladium and silver that is deposited during subsequent rounds of plating. Then, when the sample is subjected to extreme conditions, the plated layer begins to peel off of the silicon carbide. One way we had success avoiding this problem was to use a technique known as sputtering. Utilizing this technique, the peeling problem was greatly reduced and in one of our samples it did not occur at all. This success could either be attributed to smaller nuclei that were being deposited or possibly that sputtering encourages the nuclei to embed in the pores better than regular activation.

The inconsistent rate of plating led to a lot of trial-and-error when determining how long to plate for and this slowed the progress of the project. Of the three samples that were prepared, Chip 2 performed far and away the best and was the only cell to produce a voltage during final tests. The data in Table 3 shows the plating times, amounts deposited, and the ratio of Pd to Ag on the anode for each of the three chips.

Table 3: Data table of the plating results for each of the SiC supports

Anode	Chip X	Chip 1	Chip 2
Pd Coating (µm)	14.173*	6.098	2.256
Ag Coating (µm)	1.736	1.583	0.895
Total Coat (µm)	15.909	7.681	3.151
Pd:Ag Ratio	8.164	4.448	2.521
Pd Duration (min)	405	210	220
Ag Duration (min)	210	135	105
Pd:Ag Duration Ratio	1.929	1.556	2.095
Cathode			
Ag Coating (µm)	0.326*	0.00*	1.492*
Ag Duration (min)	120	60	150*

As the results show, Chip 2 was the closest to the desired ratio of Pd 77: Ag 23 and also was the most economical in the duration of plating. Several issues faced during the tests did skew the data, however. On a few tests, no mass was deposited onto the chip, yet SEM and XRD records indicated that there was some plating deposited. This may have been due to chipping off of the silicon carbide itself which counteracted the mass being gained through plating or also may have been due to a defective mass balance. This issue manifested itself in the plating results of all three samples. Also, the duration and amount of silver deposited onto the cathode of Chip 2 is misleading because 90 additional minutes were needed after running several tests because the original silver plating had been removed over time. The full chart showing each round of plating can be seen in the Appendix.

Chip X's data was altered after annealing as well, because some of the plating began to peel off. It was at this point that we switched to sputtering, which greatly reduced the peeling. In order to remove the peeling electrode, the surface was polished with 600-grit sandpaper. After polishing, the surface was sputtered and subsequent rounds of plating ensued. So while the above table does indicate the total amount of palladium and silver deposited, it is misleading because Chip X had most of its plating polished off when the peeling occurred. This left the surface unevenly plated, with some areas still having the original depositions and others stripped bare after it had peeled off. Chip 1 also succumbed to peeling, as well as rounds of plating which saw no added mass yet definitely had some deposition. Ultimately, Chip 2 had the

most success because we were able to learn from the mistakes of the other samples and was the only sample that was able to make it to the final step of actual testing.

Annealing Method

Due to the nature of the plating procedure, several alternating layers of palladium and silver are deposited on the anode face of the porous support. In order to convert these alternating layers into one uniform membrane, annealing was necessary. The purpose of annealing was to heat the sample up to the point where the lighter silver atoms diffused into the palladium layers, creating a uniform Pd/Ag alloy membrane. In order to determine the correct amount of time necessary to achieve this conversion, we used the X-Ray Diffractometer to analyze the composition of the surface. By analyzing the plot generated by Jade software, we could see the transformation from having palladium and silver to having one alloy layer. Figure 41 shows one sample's transition at three different points throughout the annealing process.

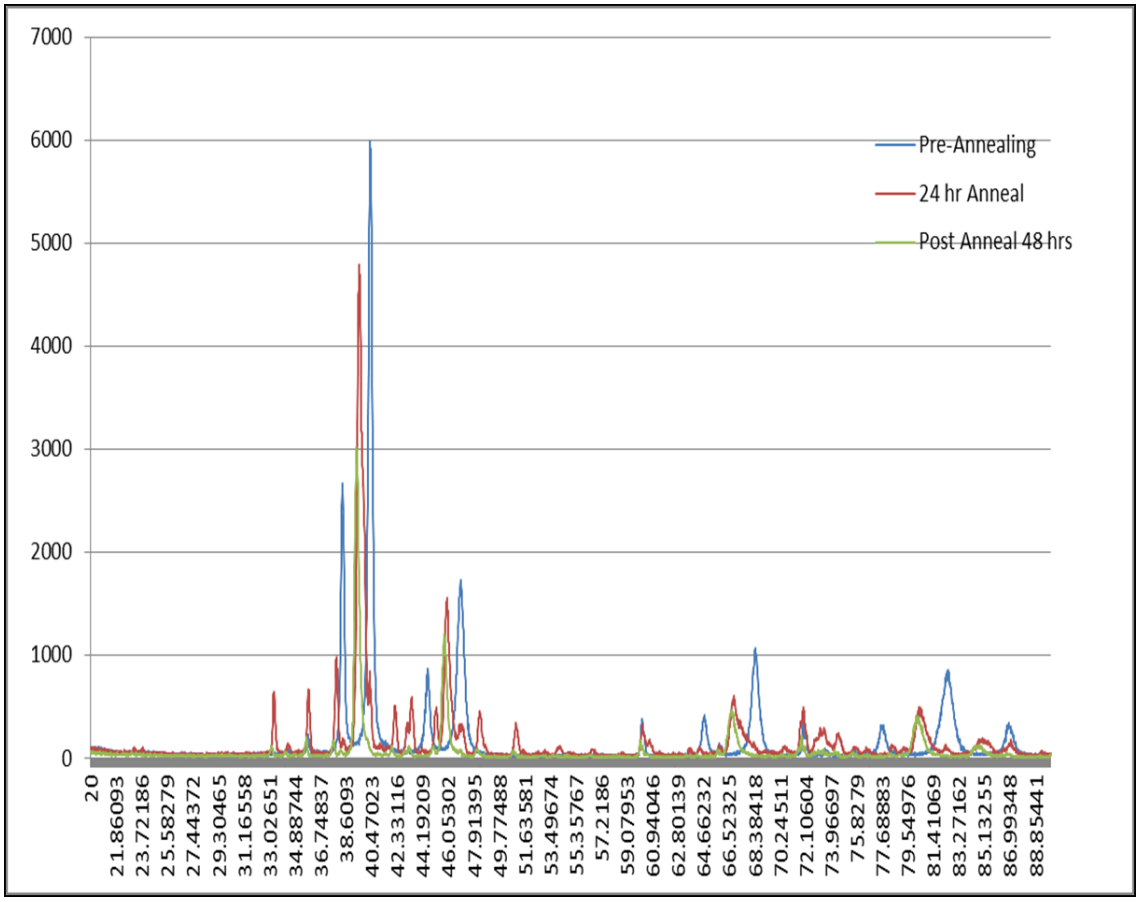

Figure 41: Overlaying plots of the XRD readings for a porous support at several stages in the annealing process

The graph is plotting the relative strength of the signal read by the XRD with the angle at which the X-rays were firing at the sample surface, which is called the 2θ value. Subtle changes in the location of the peaks indicate significant changes in the composition of the plated layer. Before annealing, there are two distinct peaks between 37 and 41 which indicate the presence of both Pd and Ag. After 24 hours of annealing, these peaks have shifted together, indicating that they are not completely separate as they were before annealing and that we were closer to getting the alloy we desired. After an additional 24 hours of annealing, the peaks shift even more and several of the smaller peaks that were visible after 24 hours of annealing have been removed. At this point it was time to evaluate the plot and determine whether we had reached our goal.

Unfortunately, these readings could not be confirmed by the Jade 8 Software because it does not have the plot for a Pd/Ag alloy in its database. By first analyzing it on Jade 8, we were able to determine that the resulting peaks no longer fit with any combination of separate palladium and silver. We then compared the XRD result to Figure 42, which is a plot for a fully annealed Pd/Ag alloy.

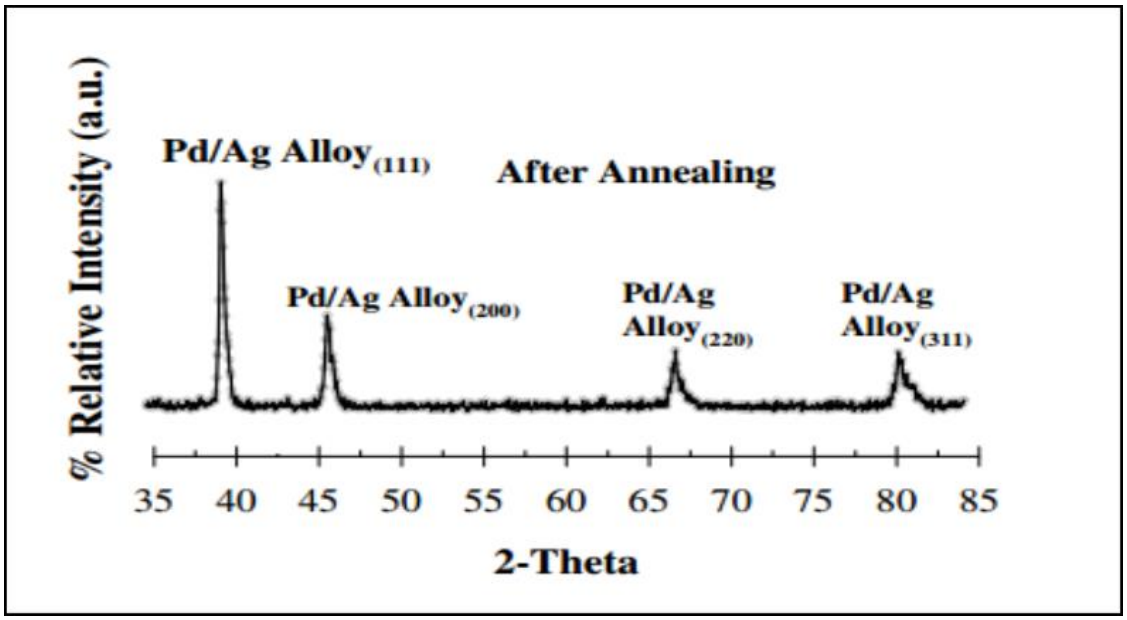

Figure 42: XRD results for a Pd/Ag alloy

Although the differences between the plots for the various stages throughout the annealing process are subtle, the 48 hour plot accurately matches this figure. Not only are the major

peaks located at the correct 2-Theta values, the small secondary peaks have also either been removed or shifted to correctly match this plot. By analyzing our samples using the XRD, we were able to determine that 48 hours of annealing at 550 ˚C in the presence of hydrogen gas is the correct method to achieve a uniform Pd/Ag alloy membrane.

Fuel Cell Performance Tests

When it came time to test our fabricated cell, only Chip 2 was ready for operation. Chip 1 had been subjected to peeling of the alloy plating and Chip X also had peeling and was cracked while the cell was being assembled. For our tests, we set the flow rates for the hydrogen gas and oxygen gas to 50 mL/min. The test station was heated to 250 ˚C to melt the catalyst. Initially, our tests did not yield results. Figure 43 shows the voltage results from our first test.

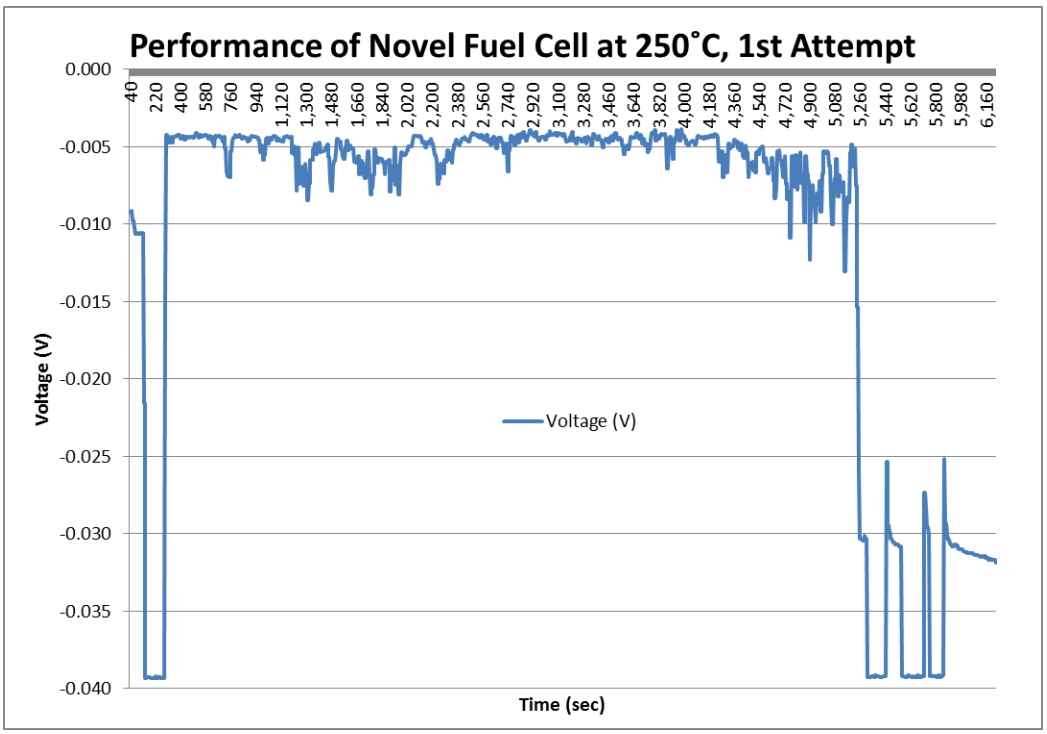

Figure 43: Failed fuel cell test likely caused by short-circuited thermocouple

As the graph shows, the cell never generated positive voltage. The negative values mostly represent error in the system, but the valleys are indicative of where the electrical senses of the test station were removed from the thermocouples to verify that the circuit was complete through the electrolyte. The zero value for the test station was -0.039 Volts.

After disassembling the cell and examining it further, it was determined that the thermocouple on the cathode side was actually short-circuiting. The short was caused by the silver paste that was used to attach the silver wire to the current-carrying wire inside of the thermocouple. This paste connected the inner wires of the thermocouple to the outer metal shell, which was in contact with the rest of the fuel cell. This meant that the circuit was not electrically insulated and it was understandable that the test station was unable to read a voltage from the fuel cell.

This thermocouple was removed from the system and replaced with a new one. We were very careful not to repeat the mistake and the thermocouple was checked multiple times to make sure that it was insulated. After reassembling the cell and renewing the test, the results were much more promising. Figure 44 shows the improved results in the second test attempt.

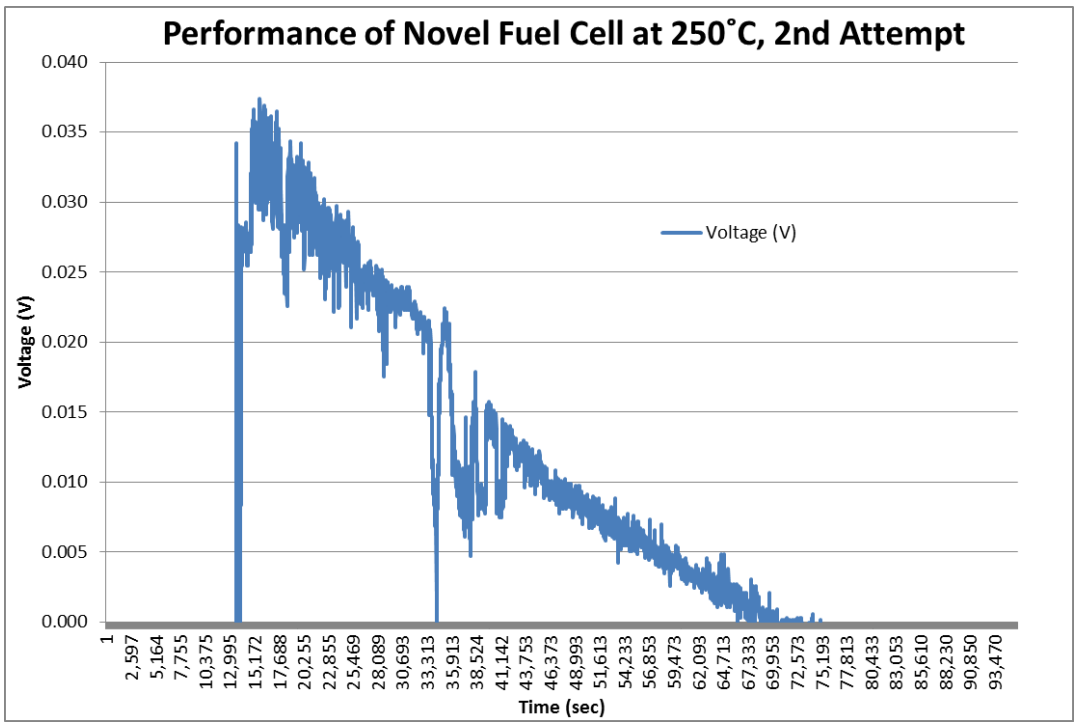

Figure 44: Fuel cell performance indicating that voltage was generated by the reactions at the electrodes

The test actually generated positive voltage this time, although still very small. On the plot, there is a significant valley that goes to zero near the 34,000 second (~9 hours). This was caused by the closing of the fuel tanks, thus cutting off the fuel to the cell. By doing this and seeing the

voltage be dependent on the flow of the fuel, it verified that the voltage was generated by the fuel cell itself and was not a result of noise from the machine.

After seeing some success with the new thermocouple, we attempted to improve the performance. To further encourage the loading of electrolyte in the support, solid chips of potassium hydroxide were placed on top of the support while it was in the reaction chamber as well as a drop of water and the test was assembled. This way the electrolyte would melt as the test heated up and only the cathode-side gas was run to possibly help push it down into the support. Running the test this way achieved the best results on our third and final test. Figure 45 shows the results for this test.

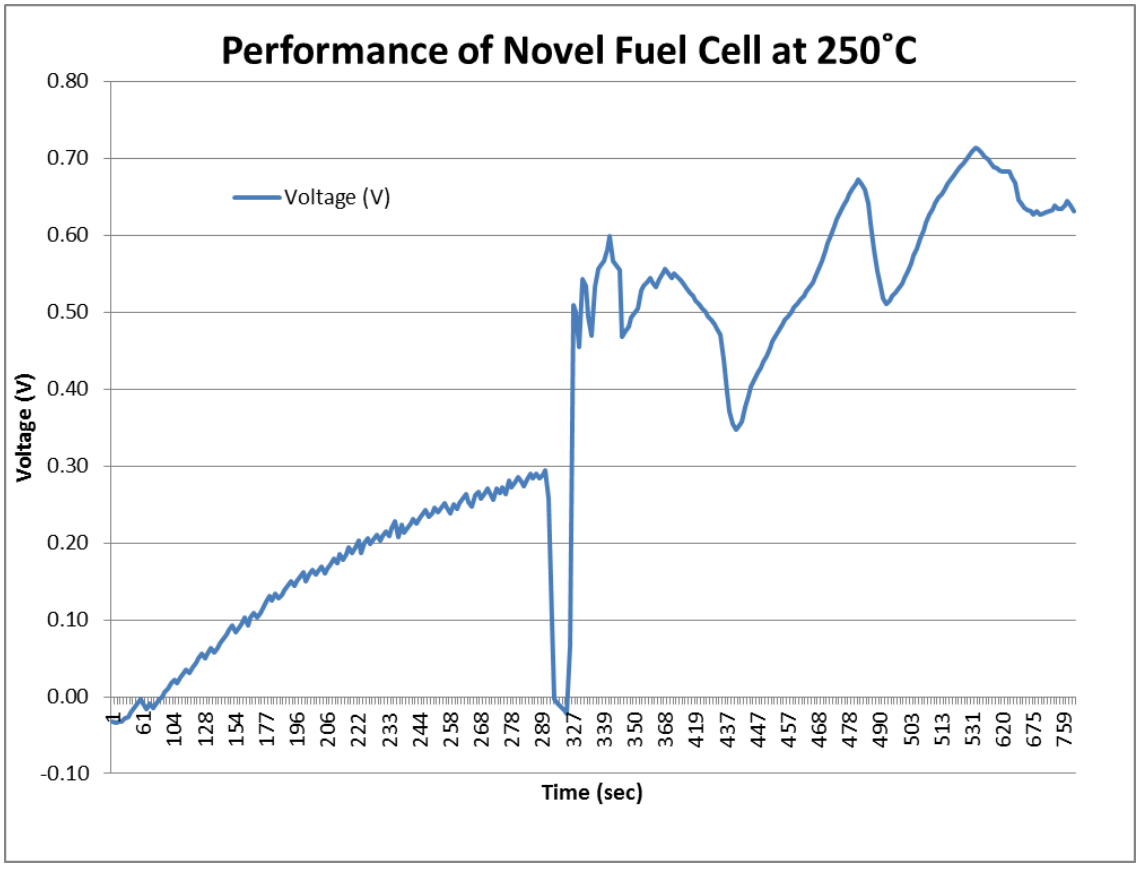

Figure 45: Performance plot showing highest voltage achieved

The peak on this plot reaches as high as 0.714 V. Although it was not holding consistent on the plot, the cell did level off and hold relatively steady at 0.68 V for approximately 5 minutes. Unfortunately, because of the inconsistent nature of the cell and concern that this may have

been our only opportunity to try, we attempted to plot a performance graph showing the voltage vs. current density and this open current voltage plot was stopped. The cell did not last for very long and by the time the voltage vs. current plot was set up, the voltage had reduced back down to below 0.1 V.

5. Conclusions & Recommendations

Going forward on this project, there is much about the fabrication process that can be improved. Preliminary tests indicate that the loading of the potassium hydroxide electrolyte into the silicon carbide support should be done at a temperature of 200 ˚C for a duration of three to six hours. This is a good temperature because it is above the melting point of the potassium hydroxide chips our project group used and tests at this temperature were more successful than those at higher temperatures. Leaving the sample in the oven for a longer period of time could result in the electrolyte reacting with the atmosphere and crystallizing. During testing, it was also found that if additional electrolyte, along with a drop of water, was placed on top of the cell while in the reaction chamber and allowed to melt into the support, the results would be much greater. It is unclear what role the water played in the success but may have helped liquefy the electrolyte. Also, it may be that the instability of the fuel cell is related to the instability of the electrolyte layer.

Further, it is recommended that sputtering be further investigated as the activation technique. One major issue encountered by this group was the peeling and flaking off of plating after annealing, and it was found that sputtering instead of using the activation solutions greatly reduced this issue. In order to reduce the inconsistencies of the plating process, the temperature of the water bath in which the plating solution sits should be allowed more time to reach equilibrium. This would add another level of stability to an unpredictable process. Also, as was said before, utilizing sputtering would help reduce the need for multiple rounds of plating because the deposited Pd and Ag would be better rooted in the support pores.

In order to create the best support for this experiment it was found that a 2:1 ratio of palladium plating to silver plating was the approximate ratio to achieve the mass ratio desired. The most successful SiC chip, Chip 2, had a ratio of 2.095. It would also be advantageous to allow the hot water bath in which the solution is submerged more time to reach equilibrium so that temperature fluctuations do not cause variations in the amount of plating per unit time.

For the annealing procedure, the best results, as determined by X-ray diffraction analyses of the sample surface, were determined to be in a hydrogen-fed oven for 48 hours for 550 ˚C. It was under these conditions that a Pd/Ag alloy membrane was made.

The generation of significant voltage across the circuit for this fuel cell was very encouraging and the progression from one test to another show that there is much room for improvement. The next step for this project is to continue testing using hydrogen while the technique for fabrication is optimized. The results generated here were promising, yet inconsistent. The recommendations made here in this report could help stabilize the performance and establish reliable trends. Once the results become more consistent, the ultimate goal of this project is to evaluate the performance of the cell using methanol as the fuel instead of pure hydrogen.

Appendix

SiC Support Plating Results – by Day

Pd Plating-Day 1						
Chip	**Wt.-Initial**	**Wt-Final**	**Wt-Pd Added**	**Density Pd**	**Surface Area**	**Pd Thickness**
(N/A)	***(grams)***	***(grams)***	***(grams)***	***(g/cm^3)***	***(cm^2)***	***(µm)***
Chip 1	0.6793	0.6796	0.0003	12.02	1.76	0.142
Chip X	0.6958	0.6987	0.0029	12.02	1.771	1.362

Pd Plating-Day 2							
Chip	**Wt.-Initial**	**Wt-Final**	**Wt-Pd Added**	**Density Pd**	**Surface Area**	**Pd Thickness**	**Total Pd**
(N/A)	***(grams)***	***(grams)***	***(grams)***	***(g/cm^3)***	***(cm^2)***	***(µm)***	***(µm)***
Chip 1	0.6796	0.6843	0.0047	12.02	1.76	2.222	2.363
Chip X	0.6987	0.7035	0.0048	12.02	1.771	2.255	3.617

Ag Plating-Day 2									
Chip	**Wt.-Initial**	**Wt-Final**	**Wt-Ag Added**	**Density Ag**	**Surface Area**	**Ag Thickness**	**Total Pd**	**Total Ag**	
(N/A)	***(grams)***	***(grams)***	***(grams)***	***(g/cm^3)***	***(cm^2)***	***(µm)***	***(µm)***	***(µm)***	**Wt. Ratio**
Chip 1	0.6837	0.6863	0.0026	10.409	1.76	1.419	2.363	1.419	1.923
Chip X	0.7011	0.7043	0.0032	10.409	1.771	1.736	3.617	1.736	2.406

Pd Plating-Day 3									
Chip	**Wt.-Initial**	**Wt-Final**	**Wt-Pd Added**	**Density Pd**	**Surface Area**	**Pd Thickness**	**Total Pd**	**Total Ag**	
(N/A)	***(grams)***	***(grams)***	***(grams)***	***(g/cm^3)***	***(cm^2)***	***(µm)***	***(µm)***	***(µm)***	**Wt. Ratio**
Chip 1	0.6863	0.6942	0.0079	12.02	1.76	3.734	6.098	1.419	4.962
Chip X	0.7043	0.706	0.0017	12.02	1.771	0.799	4.416	1.736	2.937

Ag Plating-Day 3									
Chip	**Wt.-Initial**	**Wt-Final**	**Wt-Ag Added**	**Density Ag**	**Surface Area**	**Ag Thickness**	**Total Pd**	**Total Ag**	
(N/A)	***(grams)***	***(grams)***	***(grams)***	***(g/cm^3)***	***(cm^2)***	***(µm)***	***(µm)***	***(µm)***	**Wt. Ratio**
Chip 1	0.6942	0.6945	0.0003	10.409	1.76	0.164	6.098	1.583	4.448

Pd Plating-Day 4									
Chip	**Wt.-Initial**	**Wt-Final**	**Wt-Pd Added**	**Density Pd**	**Surface Area**	**Pd Thickness**	**Total Pd**	**Total Ag**	
(N/A)	***(grams)***	***(grams)***	***(grams)***	***(g/cm^3)***	***(cm^2)***	***(µm)***	***(µm)***	***(µm)***	**Wt. Ratio**
Chip 2	0.6286	0.6295	0.0009	12.02	1.77	0.423	0.423	0	**N/A**

Chip X	0.7036	0.7073	0.0037	12.02	1.771	1.738	6.892	1.736	4.094
Pd Plating-Day 5									
Chip	**Wt.-Initial**	**Wt-Final**	**Wt-Pd Added**	**Density Pd**	**Surface Area**	**Pd Thickness**	**Total Pd**	**Total Ag**	
(N/A)	***(grams)***	***(grams)***	***(grams)***	***(g/cm^3)***	***(cm^2)***	***(µm)***	***(µm)***	***(µm)***	**Wt. Ratio**
Chip 2	0.6296	0.6333	0.0037	12.02	1.77	1.739	2.162	0	**N/A**
Ag Plating-Day 4									
Chip	**Wt.-Initial**	**Wt-Final**	**Wt-Ag Added**	**Density Ag**	**Surface Area**	**Ag Thickness**	**Total Pd**	**Total Ag**	
(N/A)	***(grams)***	***(grams)***	***(grams)***	***(g/cm^3)***	***(cm^2)***	***(µm)***	***(µm)***	***(µm)***	**Wt. Ratio**
Chip 1	0.6943	0.6943	0	10.409	1.76	0.000	6.098	1.583	**DONE**
Chip 2	0.6333	0.6338	0.0005	10.409	1.77	0.271	2.162	0.271	9.200
Ag Plating-Day 5									
Chip	**Wt.-Initial**	**Wt-Final**	**Wt-Ag Added**	**Density Ag**	**Surface Area**	**Ag Thickness**	**Total Pd**	**Total Ag**	
(N/A)	***(grams)***	***(grams)***	***(grams)***	***(g/cm^3)***	***(cm^2)***	***(µm)***	***(µm)***	***(µm)***	**Wt. Ratio**
Chip X	0.7066	0.7078	0.0012	10.409	1.77	0.651	6.892	2.061	2.977
Pd Plating-Day 6									
Chip	**Wt.-Initial**	**Wt-Final**	**Wt-Pd Added**	**Density Pd**	**Surface Area**	**Pd Thickness**	**Total Pd**	**Total Ag**	
(N/A)	***(grams)***	***(grams)***	***(grams)***	***(g/cm^3)***	***(cm^2)***	***(µm)***	***(µm)***	***(µm)***	**Wt. Ratio**
Chip X	0.7078	0.7137	0.0059	12.02	1.77	2.772	9.663	2.061	4.318
Ag Plating-Day 6									
Chip	**Wt.-Initial**	**Wt-Final**	**Wt-Ag Added**	**Density Ag**	**Surface Area**	**Ag Thickness**	**Total Pd**	**Total Ag**	
(N/A)	***(grams)***	***(grams)***	***(grams)***	***(g/cm^3)***	***(cm^2)***	***(µm)***	***(µm)***	***(µm)***	**Wt. Ratio**
Chip 2	0.6332	0.6346	0.0014	10.409	1.77	0.759	2.162	1.031	2.421
Ag Plating-Day 7									
Chip	**Wt.-Initial**	**Wt-Final**	**Wt-Ag Added**	**Density Ag**	**Surface Area**	**Ag Thickness**	**Total Pd**	**Total Ag**	
(N/A)	***(grams)***	***(grams)***	***(grams)***	***(g/cm^3)***	***(cm^2)***	***(µm)***	***(µm)***	***(µm)***	**Wt. Ratio**
Chip X	0.7055	0.7077	0.0022	10.409	1.77	1.193	9.663	3.255	2.879
Pd Plating-Day 7									
Chip	**Wt.-Initial**	**Wt-Final**	**Wt-Pd Added**	**Density Pd**	**Surface Area**	**Pd Thickness**	**Total Pd**	**Total Ag**	
(N/A)	***(grams)***	***(grams)***	***(grams)***	***(g/cm^3)***	***(cm^2)***	***(µm)***	***(µm)***	***(µm)***	**Wt. Ratio**
Chip X	0.7077	0.7173	0.0096	12.02	1.77	4.510	14.173	3.255	4.333

Pd Plating-Day 8									
Chip	**Wt.-Initial**	**Wt-Final**	**Wt-Pd Added**	**Density Pd**	**Surface Area**	**Pd Thickness**	**Total Pd**	**Total Ag**	
(N/A)	***(grams)***	***(grams)***	***(grams)***	***(g/cm^3)***	***(cm^2)***	***(µm)***	***(µm)***	***(µm)***	**Wt. Ratio**
Chip 2	0.6347	0.6349	0.0002	12.02	1.77	0.094	2.256	1.031	2.526

Ag Plating-Day 8									
Chip	**Wt.-Initial**	**Wt-Final**	**Wt-Ag Added**	**Density Ag**	**Surface Area**	**Ag Thickness**	**Total Pd**	**Total Ag**	
(N/A)	***(grams)***	***(grams)***	***(grams)***	***(g/cm^3)***	***(cm^2)***	***(µm)***	***(µm)***	***(µm)***	**Wt. Ratio**
Chip 2	0.6278	0.6303	0.0025	10.409	1.77	1.356	2.256	2.387	1.091

Bibliography

Fuel Cells. (2011). Retrieved January 24, 2013, from Methanol Institute: http://www.methanol.org/Energy/Fuel-Cells.aspx

Electrode. (2013, January 14). Retrieved January 25, 2013, from Wikipedia: http://en.wikipedia.org/wiki/Electrode#Anode_and_cathode_in_electrochemical_cells

Palladium Membrane Purification. (2013). Retrieved April 11, 2013, from PureGuard: http://pureguard.net/cm/Library/Palladium_Membrane_Purification.html

A. Tewari, V. S. (2006, January 23). Qualification of carbon dioxide poisoning in air breathing alkaline fuel cells. *Journal of Power Sources*, pp. 1-10.

C.Y. Du, T. Z. (2007, February 20). *Effect of methanol crossover on the cathode behavior of a DMFC: A half-cell investigation.* Retrieved April 11, 2013, from ScienceDirect: http://www.me.ust.hk/~mezhao/pdf/102.PDF

Carrette, L., Friedrich, K., & Stimming, U. (2001, June 27). Fundamentals and Applications. *Fuel Cells: From Fundamentals to Systems*, pp. 1-35.

Choi, W. C., Kim, J. D., & Woo, S. I. (2001). Modification of proton conducting membrane for reducing methanol crossover in a direct-methanol fuel cell. *Journal of Power Sources*, 411-414.

Datta, R. (2012). PEM Fuel Cell/ DMFC Principles. Worcester, MA, United States.

Datta, R. (2013). *Fuel Cells.* Worcester, MA.

Gernand, J. M. (2007). *Design of a Methanol to Hydrogen Micro-Reformer fr Fuel Cell Applications.* Houston, TX: Rice University.

History, N. M. (2004). *Fuel Cells*. Retrieved January 24, 2013, from Collecting the History of Fuel Cells: http://americanhistory.si.edu/fuelcells/origins/orig1.htm

Kim, T. (2009, December 1). *Micro Power Generation from Micro Fuel Cell Combined with Micro Methanol Reformer*. Retrieved February 25, 2013, from Intech: http://www.intechopen.com/books/micro-electronic-and-mechanical-systems/micro_power_generation_from_micro_fuel_cell_combined_with_micro_methanol_reformer

L. Cindrellam, A. K. (2009). Gas diffusion layer for proton exchange membrane fuel cells - A review. *Journal of Power Sources* , 146-160.

Mardilovich, P., She, Y., & Ma, Y. H. (1998). Defect-Free Palladium Membranes on Porous Stainless-Steel Support. *AIChE Journal*, 310-322.

NFCRC. (2009). *Fuel Cells Explained*. Retrieved February 20, 2013, from National Fuel Cell Research Center: http://www.nfcrc.uci.edu/2/FUEL_CELL_INFORMATION/FCexplained/FC_Types.aspx

Sameer H. Israni, M. P. (2010). Methanol Steam Reforming in Pd-Ag Membrane Reactors: Effects of Reaction System Species on Transmembrane Hydrogen Flux. *Ind. Eng. Chem. Res.* , pp. 10242-10250.

Singh, B. (2008, February 9). *Information and analysis on the economics of solar and alternative energies*. Retrieved February 20, 2013, from Green Econometrics: http://greenecon.net/hydrogen-fuel-cells-%E2%80%93-energy-conversion-and-storage/energy_economics.html

U.S. Department of Energy. (2011, March 08). *Fuel Cells*. Retrieved February 10, 2013, from Energy Efficiency and Renewable Energy: http://www1.eere.energy.gov/hydrogenandfuelcells/fuelcells/fc_types.html

U.S. Energy Information Administration. (2013, January 18). *Frequently Asked Questions*. Retrieved February 10, 2013, from Independent Statistics & Analysis: http://www.eia.gov/tools/faqs/faq.cfm?id=527&t=1

Welge, H. (1940, July). Absorption of Carbon Dioxide in Aqueous Alkalies. *Industrial and Engineering Chemistry*, pp. 970-972.

Yu-Ming Lin, M.-H. R. (2000). Process development for generating high purity hydrogen by using supported palladium membrane reactor as steam reformer. *International Journal of Hydrogen Energy*, pp. 211-219.